JSR Journal of Sedimentary Research
SEPM | Society for Sedimentary Geology

doi:10.2110/jsr.2024.124

Online 26 February 2025

Isotopic record of Aptian third-order sea-level trends in platform margin carbonates: implications for sequence stratigraphic analysis

Daniel Muñoz-López[1*], Ardiansyah Koeshidayatullah[1,2], Telm Bover-Arnal[3,4], Adhipa Herlambang[2], Juan Diego Martín-Martín[3,4], Ramon Salas[3,4], John D. Humphrey[1], Khalid Al-Ramadan[1,2*].

[1]Department of Geosciences. College of Petroleum Engineering and Geosciences. King Fahd University of Petroleum and Minerals, Dhahran, 31261. Saudi Arabia

[2]Center for Integrative Petroleum Research. College of Petroleum Engineering and Geosciences. King Fahd University of Petroleum and Minerals, Dhahran, 31261. Saudi Arabia

[3]Departament de Mineralogia, Petrologia i Geologia Aplicada, Facultat de Ciències de la Terra, Universitat de Barcelona, Martí i Franquès s/n, 08028 Barcelona, Spain

[4]Institut de Recerca GEOMODELS. Martí i Franquès s/n, 08028 Barcelona, Spain.

ABSTRACT

In ancient carbonate systems, establishing relationships among sea-level fluctuations, carbonate factory productivity and carbonate geochemistry is challenging due to complex depositional and diagenetic overprinting. The Aptian platform carbonate succession from the western Maestrat Basin, in Spain, serves as an ideal example for potentially linking these processes, particularly establishing the relationships between isotopic records ($\delta^{18}O$ and $\delta^{13}C$) and third-order sea-level trends with implications for sequence stratigraphy. This succession is biostratigraphically well-constrained and comprises two depositional sequences that were controlled by a major relative sea-level fall and a subsequent rise. These depositional sequences exhibit stratal terminations and stacking patterns, enabling the establishment of a well-defined sequence stratigraphic framework comprising four systems tracts and their key bounding stratigraphic surfaces. The analytical

results reveal that both $\delta^{18}O$ and $\delta^{13}C$ values outline distinct temporal trends, which can be correlated with specific third-order stages of relative sea-level fluctuations. The transgressive and highstand systems tracts exhibit the most positive $\delta^{13}C$ values (up to +5‰) and the least negative $\delta^{18}O$ values (up to -1.8‰). This range, similar to values of carbonates in equilibrium with Cretaceous seawater, $\delta^{13}C$ and $\delta^{18}O$ values from +2‰ to +5‰ and from -2‰ to -5‰, respectively, likely reflects the marine influence on the isotope values during the stage of high relative sea level. In contrast, the forced regressive and lowstand intervals exhibit less positive $\delta^{13}C$ values (reaching +0.5‰) and significantly more negative $\delta^{18}O$ values (around -6.1‰), interpreted as the influence of soil-derived organic matter and meteoric waters, respectively, during stages of lower relative sea level. Furthermore, the sedimentary succession records a decreasing trend of $\delta^{13}C$ and $\delta^{18}O$ values towards the sequence boundary, which marks the lowest point of relative sea level. This study underscores the potential of carbonate platforms to record geochemical signals that can be directly correlated with different third-order stages of relative sea-level variations. In addition, this framework allows for linking and predicting the potential fluid-rock interaction processes in each systems tract. The proposed approach could offer a predictive framework for characterizing carbonate reservoirs and other carbonate platform successions with poorly defined sequence-stratigraphic frameworks elsewhere.

Keywords: Stable Isotopes; Geochemistry; Sequence Stratigraphy; Sea-level Fluctuation; Carbonates

INTRODUCTION

Third-order relative sea-level fluctuations (sensu Vail et al., 1991) play a pivotal role in controlling physical and ecological accommodation and influencing the nature and architecture of depositional facies in platform carbonates (Eberli, 2000; Anselmetti et al., 2000). The

interplay between sedimentation and accommodation defines the sequence stratigraphic framework and exerts control over the extent and distribution of depositional and diagenetic alterations that impact the sedimentary succession during and after deposition (Schlager, 2005; Catuneanu et al., 2009). Given that many factors influencing carbonate geochemistry, such as pore water chemistry, depositional setting, and burial/exposure, are also sensitive to changes in relative sea level, isotope geochemistry can be directly linked to sequence stratigraphy (Tucker, 1993; Weissert et al., 1998; Spezzaferri et al., 2002; Burla et al., 2008; Mehrabi et al., 2022). Correlations between carbon isotopic values and changes in relative sea level, with implications for sequence stratigraphy, have already been noticed in contributions studying pelagic and shallow-water carbonates (Föllmi et al., 1994; Vahrenkamp, 1996; Eberli, 2000; Saltzman, 2002; Spezzaferri et al., 2002; Immenhauser et al., 2003; Krull et al., 2004). However, in some case studies, including the Holocene to Early Miocene record of the Bahamas, $\delta^{13}C$ values of platform and periplatform sediments were unrelated to synchronous shifts in the $\delta^{13}C$ of the open oceans. This was interpreted to indicate that $\delta^{13}C$ trends of these sediments did not correlate with the ocean-climatic system (or the global $\delta^{13}C$ signal) over this time period (Swart and Eberli, 2005). In the Arabian Gulf, however, the $\delta^{13}C$ patterns of Lower Cretaceous shallow-water carbonates were controlled by third-order fluctuations in relative sea level and correlated with isotopic profiles reported elsewhere in Tethyan pelagic limestones of the same age (Föllmi et al., 1994; Vahrenkamp, 1996). This led to the suggestion that the isotopic proxy was an effective tool for characterizing relative sea-level fluctuations in the lower Cretaceous record of the Arabian (Tethyan?) region (Vahrenkamp, 1996). Similar conclusions, suggesting comparable $\delta^{13}C$ shifts in carbonate lithofacies from different water depths, were obtained in Mississippian carbonates from western USA (Saltzman, 2002, 2003). The later authors placed the carbonate $\delta^{13}C$ and $\delta^{18}O$

variations in a sequence stratigraphic framework to evaluate the presence of exposure surfaces and to distinguish between primary and secondary stable isotope patterns (Saltzman, 2002).

Despite this good correlation between isotope stratigraphy and relative sea-level fluctuations in carbonate environments, linking chemostratigraphic data to sequence stratigraphic concepts have proven effective mostly in siliciclastic systems (Haq et al., 1987; Posamentier et al., 1992; Morad et al., 2000, 2010, 2013; Al-Ramadan et al., 2005). This is due to the wide variety and complexity of carbonates resulting from the interaction among relative sea-level changes, local tectonics, climate, type of biota, diagenesis, and heterogeneous mineralogy and texture (Gischler et al., 2009; Pomar and Haq, 2016). Besides, recognizing or interpreting sequence stratigraphic attributes in ancient carbonate environments can also be challenging due to poor exposure conditions, variable rates of erosion and sedimentation, and superposition of different stratigraphic surfaces (Immenhauser et al., 2002; Christ et al., 2012). In such cases, data gaps are addressed by incorporating interpreted surfaces that introduce greater uncertainty to the interpreted stratigraphic model (Catuneanu et al., 2009).

Carbonate platform margins represent the best setting to estimate fluctuations in relative sea level and to evaluate the global versus local controls on platform evolution (Pomar et al., 2005). A modern setting, often applied as analogue of ancient platform carbonates, comes from the Great Bahama Bank (GBB) and its subsurface sediments (Eberli, 2000; Anselmetti et al., 2000; Eberli et al., 2002; Spezzaferri et al., 2002; Reuning et al., 2006; Reijmer et al., 2009; Murray and Swart, 2017; Murray et al., 2021). However, the question that commonly arises is whether the results, in terms of facies distribution, mineralogy and geochemistry, are applicable to all geological time periods (Swart et al., 2009). In the case of ancient carbonates, the Guadalupian outcrops of the Permian Basin (USA) provide a classic example of a large and continuous

exposure illustrating the architecture and sequence stratigraphy of a self-to-basin section (Harris and Saller, 1999).

In this contribution, we focus on the Aptian "Las Mingachas" section in the western marginal part of the Maestrat rift basin (Iberian Chain) in Spain. This section stands out as one of the very few outcrops worldwide that preserves stacking patterns and stratal terminations that permit one to define sequence stratigraphic surfaces that bound different systems tracts (Bover-Arnal et al., 2009, 2022). In general, Las Mingachas section exhibits stratigraphic continuity, with its age calibrated using Sr-isotope stratigraphy, as well as ammonite, orbitolinid, and rudist biostratigraphies (Moreno-Bedmar et al., 2010; Bover-Arnal et al., 2016). Furthermore, Las Mingachas section offers an exceptionally well-preserved platform-to-basin transition, showing sedimentary evidence of the influence of third-order relative sea-level fluctuations, including a major sea-level fall and a subsequent rise, on carbonate sedimentation across the system (Bover-Arnal et al., 2009, 2022). Thus, drawing upon this well-established sequence stratigraphic framework, this contribution provides carbonate geochemical measurements at Las Mingachas section aiming to: i) test if the stable carbon and oxygen isotopes of the Aptian platform carbonates are in line with the interpreted sequence-stratigraphic framework and the reported third-order fluctuations in relative sea level, especially considering the nature of the major sea-level fall, interpreted to be of global significance with a dominant eustatic contribution; ii) verify if this geochemical record enables the identification of the attributes of a four systems tracts-based sequence stratigraphic framework (Hunt and Tucker, 1992), which is a complete framework not commonly preserved in the stratigraphic record; and (iii) to corroborate if the new provided data allows us to discern between divergent interpretations concerning part of the stratigraphic framework reported in the study area (Bover-Arnal et al., 2009, 2022; Peropadre et

al., 2013; Pomar and Haq, 2016; Pomar, 2020). Thus, this case study exemplifies an ideal scenario to assess the robustness of stable isotope proxies in identifying Aptian third-order sea-level trends and geochemically characterizing the complete "four-systems-tract" sequence stratigraphic model of Hunt and Tucker (1992).

GEOLOGICAL SETTING

The studied Aptian carbonate succession is located in the eastern part of the Iberian Chain in Spain (Fig. 1), which is an intraplate fold-and-thrust belt that resulted from the Alpine (late Eocene-early Miocene) tectonic inversion of the Mesozoic Central Iberian Rift System (Salas & Casas, 1993; Salas et al., 2001; Guimerà et al., 2004). Late Jurassic and Early Cretaceous rifting stages in Iberia were linked to the opening of the North Atlantic Ocean and the Bay of Biscay, respectively. These two rifting stages gave rise to major NW-SE, E-W and NE-SW normal faults that controlled the formation of rapidly subsiding basins, including the Maestrat Basin, which is the focus of this study (Salas et al., 2001). The selected outcrops are located in a western marginal area of the Maestrat Basin known as the Galve sub-basin (Fig. 1) (Liesa et al., 2006; Salas et al. in Martín-Chivelet et al., 2019). The stratigraphic interval analyzed corresponds to a platform-to-basin transition area known as "Las Mingachas" (Figs. 1 & 2) and spans the late early-earliest late Aptian time slice (Moreno-Bedmar et al., 2010; Bover-Arnal et al., 2016, 2022). This marine succession postdates the early Aptian oceanic anoxic event (OAE1a) (Bover-Arnal et al., 2010). The Las Mingachas section comprises the upper part of the long-term T-R Sequence II and the lower part of T-R Sequence III described in Bover-Arnal et al. (2010, 2016). The following description of facies and the sequence stratigraphic framework is based on Bover-Arnal et al. (2009, 2022).

Sequence Stratigraphic Framework

The transition zone from platform to basin at Las Mingachas was interpreted within a sequence stratigraphic framework consisting of four systems tracts, encompassing two depositional sequences: A and B. Depositional Sequence A includes a Highstand Systems Tract (HST) and a Forced Regressive Wedge Systems Tract (FRWST). In contrast, Depositional Sequence B is composed of a Lowstand Prograding Wedge Systems Tract (LPWST), a Transgressive Systems Tract (TST), and the subsequent HST (Figs. 2 & 3).

HST (Depositional Sequence A).---

The first HST consists of a carbonate platform comprising corals and rudists belonging to the Villarroya de los Pinares Formation, which shows aggrading and subsequent prograding patterns. Towards the basin, located in the SW of the study area, the platform top limestones pass to slope deposits, which exhibit downlapping stratal terminations and laterally pass into the marls of the Forcall Formation (Fig. 2). The downlap surface separates the upper limestones with corals and rudists from lower, deeper basinal marls, thus representing the maximum flooding surface (MFS) of Depositional Sequence A (Bover-Arnal et al., 2009). The basinal marls, equivalent to the platform's top limestones, are interpreted as part of the highstand normal regressive unit, whereas the marly deposits below the MFS are considered a transgressive succession. These basinal marly deposits correspond to the Forcall Formation.

FRWST (Depositional Sequence A).---

The FRWST is represented by a high energy regressive wedge constituted by cross-bedded grainstones occurring basinwards, at the toe of highstand slopes. These calcarenite deposits belong to the Villarroya de los Pinares Formation, and are made up of an autochthonous carbonate factory dominated by oysters, and of allochthonous lithoclasts that resulted from

erosion of the exposed carbonate platform during a sea-level fall that was estimated to be of at least 60 meters (Bover-Arnal et al., 2009). The lower boundary of the calcarenite deposits, i.e., the basal surface of forced regression (BSFR), is represented by a sharp surface separating the underlying basinal highstand marls of the Forcall Formation from the overlying shallower forced regressive wedge. In turn, the upper boundary of the regressive wedge is represented by the sequence boundary (SB), which separates depositional sequences A and B and marks the lowest point of relative sea level. The SB is characterized by a subaerial unconformity that becomes younger seawards, passing to a marine correlative conformity (CC) over the FRWST (Fig. 2).

LPWST (Depositional Sequence B).---

The LPWST consists of a small carbonate platform dominated by corals and rudists that shows a progradational stacking pattern followed by aggradation (Fig. 2). The lowstand platform, which developed during the subsequent base-level rise, is also part of the Villarroya de los Pinares Formation. The platform top facies pass into slope deposits basinwards. The upper boundary of the lowstand unit is marked by the transgressive surface (TS), which corresponds to a hardground with *Lithophaga* borings and iron mineralization. Landwards, the TS superimposes the SB and therefore, the subaerial unconformity that separates the two depositional sequences becomes a composite sequence boundary (i.e., SB + TS).

TST (Depositional Sequence B).---

In Las Mingachas, the TST corresponds to retrograding platform top carbonates with rudists and corals that onlap the composite sequence boundary between Depositional Sequences A and B (SB + TS) towards the land (Fig. 2). The backstepping limestones change basinwards into marly deposits of the lower part of the Benassal Formation, and also upwards in the succession after

183 drowning of the Villarroya de los Pinares platform. The maximum flooding surface (MFS) of
184 Depositional Sequence B is interpreted to be located at the top of the thickest marl bed of the
185 lower part of the Benassal Formation, coinciding with the downlap surface of overlying coral-
186 bearing deposits.

187 **HST (Depositional Sequence B).---**

188 The succeeding highstand deposits also belong to the Benassal Formation (Fig. 2) and are
189 characterized by platform carbonates with corals, rudists and nerineid gastropods. Above the
190 MFS of Depositional Sequence B, the basal part of this highstand unit is characterized by a
191 marly horizon with irregular and massive corals, alternating with limestone beds of carbonate
192 shed from platform top settings.

193 ## METHODOLOGY

194 This study includes stable isotope measurements ($\delta^{13}C$ and $\delta^{18}O$ values) of the Aptian carbonate
195 platform cropping out at Las Mingachas section. Previous research established the facies
196 architecture, as well as the paleoenvironmental and sequence stratigraphic interpretation,
197 including the reconstruction of the relative sea-level stages based on stratigraphic data (Bover-
198 Arnal et al., 2009, 2022). This previous research guided the selection of outcrops and samples to
199 conduct geochemical analyses. The selected outcrop corresponds to the platform-to-basin
200 transition area of Las Mingachas section, where the sedimentary succession includes four
201 systems tracts encompassing two depositional sequences (Fig. 2). In this area, a representative
202 log was measured, and facies variations, along with key stratigraphic surfaces, were mapped on a
203 panoramic view and correlated with the surfaces described in previous studies of the area (Fig.
204 3). Ninety samples were collected in the field following two sampling strategies for comparison.

205 "LM samples" cover laterally the full platform to basin transition area shown in Figures 2 and 3
206 (i.e., covering the entire platform and throughout all systems tracts), whereas "vertical log
207 samples" were taken vertically next to the stratigraphic log (Fig. 3). Thus, collected samples
208 cover along dip and along strike the full outcrop from the uppermost slope and towards the basin,
209 where the subaerial unconformity, representing the composite sequence boundary, passes to its
210 marine correlative conformity (Fig. 2A).

211 LM samples were prepared for stable isotope measurements ($\delta^{13}C$ and $\delta^{18}O$) of bulk carbonates
212 and separate carbonate components (micritic matrix, grains, and cements), whereas, in vertical
213 log samples, only bulk carbonates were analyzed. In total, this study provides fifty-nine analyses
214 of bulk carbonates and thirty-one analyses of separate carbonate components.

215 Bulk carbonates and separate carbonate components (micritic matrix, grains, and cements) of
216 LM samples were sampled using a microdrill to extract carbonate powder (n=49). Powdered
217 samples (50-60 μg) were reacted at 70°C with 102–105% phosphoric acid before CO_2 gas was
218 liberated to the automated purification line. Then, the product CO_2 was purified using cryogenic
219 traps to eliminate contaminant gases, such as water vapor and non-condensable gases produced
220 during the acid digestion of the carbonate samples. Purification was performed automatically
221 using a Kiel IV carbonate device. The CO_2 gas released was analyzed with a Thermo Scientific
222 MAT 253+ mass spectrometer at the Stable Isotope Laboratory, King Fahd University of
223 Petroleum and Minerals (Dhahran, Saudi Arabia) with an overall precision of 0.08‰ for $\delta^{18}O$
224 and 0.04‰ for $\delta^{13}C$, as measured by blind sample replicates. The oxygen and carbon isotope
225 data are presented in δ notation relative to the Vienna Pee Dee Belemnite (VPDB) standard via
226 standard reference materials obtained from the US National Institute of Standards and
227 Technology and the International Atomic Energy Agency.

The measurements on a mass spectrometer drift over time for several reasons, including ion source performance (D'Autry et al., 2010) or the presence of contaminants. The drift was corrected by plotting the raw $\delta^{18}O$ and $\delta^{13}C$ data against the internal laboratory carbonate standard (KIS; KFUPM Iceland Spar) with the accepted isotopic values of 2.25‰ and -6.23‰ (VPDB) for $\delta^{13}C$ and $\delta^{18}O$, respectively.

Bulk vertical log samples, encompassing limestones, marly limestones, and marls were also analyzed for $\delta^{13}C$ and $\delta^{18}O$ measurements (n=41). For each analysis, 60-70 μg of material was used for limestones, while marls and marly limestones were analyzed with quantities ranging from 100-1000 μg. To extract carbonate powder from limestones and avoid large skeletal components, corals, microencrusters or diagenetic calcite veins, a microdrill was employed. The samples underwent treatment with H_3PO_4 (100%) at 70°C, and the evolved CO_2 was analyzed using a Thermo Finnigan MAT-252 stable isotope ratio mass spectrometer at the Scientific and Technological Centers of the University of Barcelona. The isotope results are expressed in ‰ relative to the VPDB standard, with a precision of ±0.03 for $\delta^{13}C$ and ±0.06 for $\delta^{18}O$.

RESULTS

Sedimentary succession logged and sampled

The analyzed stratigraphic section is representative of the two identified depositional sequences, A and B, and the three sedimentary formations: Forcall, Villarroya de los Pinares and Benassal (Fig. 3). This section commences with alternating marls, marly limestones and limestones, which are attributed to the uppermost part of the Forcall Formation (Fig. 3 & 4A). These marly deposits between meters 0 and 15 represent the highstand deposits of Depositional Sequence A (Bover-Arnal et al., 2009, 2022). The marly limestones and limestones exhibit mudstone to packstone

textures and contain skeletal components such as *Palorbitolina lenticularis* (Fig. 4B), calcareous dinoflagellate cysts, textularids, miliolids, ammonoids, sponge spicules, brachiopods, and echinoids, whereas the non-skeletal components mainly consist of peloids and quartz grains. Towards the north (i.e., landwards, in higher topographic areas), this marly interval passes to an aggrading to prograding carbonate platform that exhibits downlap stratal terminations. These highstand platform carbonates are attributed to the Villarroya de los Pinares Formation and consist of limestones showing floatstone to rudstone textures made up of rudist and corals in life position.

Above the marly deposits of the Forcall Formation, there are packstone to grainstone limestones, displaying low-angle crossbedding. These rocks are characterized by the occurrence of conical *Orbitolinopsis* (Fig. 4C), calcareous algae *Permocalculus* and *Marinella lugeoni*, fragments of corals, and intraclasts. These deposits of the Villarroya de los Pinares Formation, between metres 15 and 19, constitute the FRWST of Depositional Sequence A (Fig. 3; see Bover-Arnal *et al*., 2009, 2022). At meter 19, a sharp stratigraphic surface marks the top of the FRWST. This surface, which is downlapped by lowstand slope deposits has been interpreted as the lowest point of relative sea level, marking the sequence boundary (SB) (Bover-Arnal et al., 2009, 2022). Landwards, the SB is truncated and exhibits paleokarst features and thus, it is classified as a subaerial unconformity (SU). Within the uppermost slope and towards the basin, the SB does not show evidence of subaerial exposure and thus, it is classified as a marine correlative conformity (CC). Between meters 19 and 43 the Villarroya de los Pinares Formation succession is made up of an alternation between marls, which contain scleractinian colonies in growth position, and limestones with rudstone to floatstone textures with rudist shells, corals, and *Permocalculus* (Fig. 4D). Limestones show a prograding and then an aggrading pattern and exhibit downlap stratal

terminations. Consequently, Bover-Arnal *et al.* (2009, 2022) interpreted this stratigraphic interval as a LPWST belonging to Depositional Sequence B (Fig. 3).

The upper part of the Villarroya de los Pinares Formation, between meters 43 and 46, corresponds to limestones showing a floatstone to rudstone texture (Fig. 4E). These strata are dominated by colonial corals, rudists such as *Toucasia carinata* and *Polyconties hadriani*, *Chondrodonta*, *Permocalculus*, and nerineid gastropods. This interval represents the early TST of Depositional Sequence B (Figs. 2 & 3; Bover-Arnal *et al.*, 2009, 2022), and exhibits a backstepping geometry that is topped by a hardground with borings made by lithophagid bivalves and ferruginous stains (see Figs. 8E-F in Bover-Arnal et al., 2022). Above, from meter 46 until the end of the measured section, a marly succession characterized by the presence of large gastropods of the species *Trochoneritas gigas* overlies the platform carbonates of the Villarroya de los Pinares Formation. This marly stratigraphic interval was interpreted as the upper part of the TST of Depositional Sequence B (Bover-Arnal *et al.*, 2009, 2022) and constitutes the lower part of the Benassal Formation (Figs. 2 & 3). Given the absence of sedimentary or biotic indicators of bathymetry, the maximum flooding surface (MFS) of Depositional Sequence B was placed at the top of the thickest marl unit within the TST. Above this surface, the marly deposits evolve into slope facies, characterized by marls containing isolated coral colonies. The slope deposits pass upwards into platform top carbonates made up of floatstones and rudstones with corals, rudists, and nerineid gastropods. These slope to platform top facies represent the HST of Depositional Sequence B (Bover-Arnal et al., 2009).

Carbon and oxygen isotopes

Stable carbon and oxygen isotopic values of the studied Aptian platform carbonates vary widely from +0.5‰ to +5.3‰ and from -6.2‰ to -1.8‰, respectively (Table 1 and Figs. 5 & 6).

296 Overall, the $\delta^{13}C$ curve displays a distinctive pattern characterized by two intervals of persisting
297 positive carbon isotopic values (+4‰ ± 1‰ approx.) separated by a negative carbon isotopic
298 excursion of around 4‰. Likewise, with a greater dispersion of values, the $\delta^{18}O$ curve shows a
299 negative oxygen isotopic excursion, reaching -6‰, separating two intervals of less negative (but
300 widely varying) oxygen values (Figs. 5 & 6).

301 Furthermore, despite the slight overlap between some samples, each studied systems tract
302 exhibits a distinctive range of isotopic values. This range does not vary laterally within the same
303 systems tract (i.e., we do not observe along strike isotopic patterns within the same genetic type
304 of deposits). Instead, the isotopic trends vary vertically (i.e., isotopic values increasing or
305 decreasing from one systems tract to another), as explained below.

306 **HST (Depositional Sequence A).---**

307 In LM samples, bulk carbonates from the first HST exhibit $\delta^{13}C$ and $\delta^{18}O$ values ranging from
308 +2.6‰ to +4.7‰ and from -5.3‰ to -3.2‰, respectively, whereas carbonate components vary in
309 $\delta^{13}C$ and $\delta^{18}O$ values from +3.6‰ to +4.7‰ and from -5.7‰ to -4.4‰, respectively (Table 1 and
310 Figs. 5 & 6). In vertical log samples, these HST bulk carbonates show $\delta^{13}C$ and $\delta^{18}O$ values from
311 +3.2‰ to +5.1‰ and from -3.7‰ to -3.1‰, respectively.

312 **FRWST (Depositional Sequence A).---**

313 Compared to the HST, the FRWST interval shows an overall trend towards less positive and
314 more negative carbon and oxygen isotope values, respectively (Table 1 and Figs. 5 & 6). That is,
315 LM bulk carbonate samples from this interval yield average $\delta^{13}C$ values of +0.9‰ and $\delta^{18}O$
316 values of -5.7‰, whereas carbonate components have $\delta^{13}C$ and $\delta^{18}O$ values from +0.5‰ to
317 +3.5‰ and from -6.0‰ to -5.6‰, respectively. These values are within the range of values

obtained in FRWST bulk carbonates from vertical log samples, where $\delta^{13}C$ and $\delta^{18}O$ values vary from +0.8‰ to +4.2‰ and from -6.0‰ to -3.6‰, respectively. In the $\delta^{13}C$ and $\delta^{18}O$ profiles of the FRWST interval, both carbon and oxygen isotopic values generally decrease vertically (upwards) from the lower (BSFR) to the upper (CC) stratigraphic surface (Figs. 5 & 6). This means that carbon and oxygen values progressively shift from around +4.0‰ and from -4.0‰, respectively in the BSFR, to +0.5‰ and -6‰, respectively, in the CC.

LPWST (Depositional Sequence B).---

The LPWST has a similar range of values to the FRWST interval (Table 1 and Figs. 5 & 6). That is, bulk carbonates in LM samples display $\delta^{13}C$ and $\delta^{18}O$ values from +1.7‰ to +4.1‰ and from -5.2‰ to -4.7‰, respectively, whereas carbonate components show $\delta^{13}C$ and $\delta^{18}O$ values from +1.2‰ to +4.5‰ and from -6.1‰ to -3.7‰, respectively. Again, bulk vertical log samples in LPWST yield similar $\delta^{13}C$ and $\delta^{18}O$ values, between +1.3‰ and +4.1‰ and between -6.1‰ and -3.5‰, respectively. Overall, $\delta^{13}C$ and $\delta^{18}O$ values progressively increase vertically from the lower to the upper surface of the LPWST interval, that is, from the CC towards the TS (Figs. 5 & 6).

TST (Depositional Sequence B).---

LM Bulk carbonate samples from the TST exhibit $\delta^{13}C$ and $\delta^{18}O$ values from +2.5‰ to +5.1‰ and from -5.9‰ to -3.7‰, respectively, whereas carbonate components vary in $\delta^{13}C$ and $\delta^{18}O$ values from +3.5‰ to +5.3‰ and from -6.2‰ to -2.3‰, respectively (Table 1 and Figs. 5 & 6). Similar values have been measured in bulk vertical log samples for TST, which yield $\delta^{13}C$ and $\delta^{18}O$ values between +1.3‰ and +5.2‰ and between -5.7‰ and -2.4‰, respectively.

HST (Depositional Sequence B).---

This carbonate interval has only been sampled in LM samples (Table 1 and Figs. 5 & 6). The bulk carbonate sample shows $\delta^{13}C$ values of +3.6‰ and $\delta^{18}O$ values of -1.8‰, whereas carbonate components have $\delta^{13}C$ values of +4.4‰ and $\delta^{18}O$ values of -3.9‰.

DISCUSSION

Linking third-order sea-level trends to carbonate stable isotopes

The sequence stratigraphic framework of the Aptian platform margin studied here was arranged into two depositional sequences (A and B) that formed as a result of a major fall and a subsequent rise in relative sea level, respectively (Fig. 2; Bover-Arnal et al., 2009, 2022). Carbonate production and accumulation during the late early-early late Aptian was closely linked to these relative sea-level fluctuations (Bover-Arnal et al., 2009; Gratacós et al., 2021). Consequently, the isotopic patterns recorded in these platform carbonates may be used to reconstruct not only the depositional setting but also the superposed changes in relative sea level and its associated fluid-rock interactions (e.g., Swart & Eberli, 2005; Vahrenkamp, 1996).

The two observed intervals in the $\delta^{13}C$ and $\delta^{18}O$ profiles showing the most positive carbon values (+4‰ ± 1‰ approx.) and the less negative (and less varying) oxygen values (-5.5‰ to -3‰) coincide with two specific stages of relative sea-level high: HST of Depositional Sequence A and TST-HST of Depositional Sequence B (Figs. 5 & 6). These more positive $\delta^{13}C$ and less negative $\delta^{18}O$ values are within the range of carbonates in equilibrium with Cretaceous seawater, which typically display $\delta^{13}C$ and $\delta^{18}O$ values ranging from around +2‰ to +5‰ and from -2‰ to -5‰, respectively (Veizer et al., 1999). The correspondence between isotopic values recorded in highstand and transgressive intervals, and those typical values of contemporaneous seawater is interpreted to reflect the marine influence on the carbonate isotope values during the maximum

relative sea-level high (D'Argenio et al., 2004; Föllmi et al., 2006). During periods of high relative sea level, the continental shelf is flooded and the carbonate factory produces carbonate at its maximum activity, leading to high amounts of organic carbon burial (Magaritz, 1989). In turn, the increase in carbon burial rates enhances removal of light carbon from the ocean-atmosphere system by burial of ^{13}C-depleted organic matter (Jenkyns, 1996; Gröcke et al., 1999; Jarvis et al., 2001, 2002). A high rate of carbonate production during the HST of Depositional Sequence A is evidenced by the abundance of lime mud present, the diversity of carbonate producers, including corals and rudists in life position and nerineid gastropods, and the metric thickness of beds that characterize this systems tract (Bover-Arnal et al., 2009). The high carbonate accumulation rate during the slowing sea-level rise, typical of the HST, notably reduced accommodation in the late HST. This interpretation is supported by the observed prograding stacking pattern exhibited by the HST. In contrast, during the TST of Depositional Sequence B, the carbonate accumulation rate was outpaced by the rate of relative sea-level rise. As a result, the carbonate platform, displaying a retrograding pattern, was eventually drowned. This is evidenced by the sedimentary succession passing upwards into marly deposits (Fig. 3). The observed geochemical behavior agrees with similar conclusions elsewhere suggesting that positive carbon isotope excursions are associated with maximum relative sea-level highs and vice versa (D'Argenio et al., 2004; Swart and Eberli, 2005; Föllmi et al., 2006).

The second observed trend in the isotopic profiles shows a decrease in $\delta^{13}C$ and $\delta^{18}O$ values in the FRWST interval of Depositional Sequence A (i.e., coinciding with the stage of base-level fall). In this regressive interval, $\delta^{13}C$ and $\delta^{18}O$ values progressively decrease from the BSFR towards the SB (correlative conformity), shifting from +4‰ to around 0‰ and from -4‰ to -6‰, respectively (Figs. 5 & 6). Therefore, this lowering isotopic values during the falling

relative sea level is here interpreted to reflect the gradual exposure of the platform top to subaerial conditions (Figs. 2-3 & 5-7). Through water-rock interaction under subaerial conditions: (i) the $\delta^{18}O$ values are usually lowered by isotopically light meteoric fluids, which have lower $\delta^{18}O$ values than seawater values, whereas the $\delta^{13}C$ values are lowered by the increasing influence of CO_2 derived from the soil zone and the oxidation of organic matter (Allan and Matthews, 1977; Popp et al., 1986; Sattler et al., 2005); and (ii) the previously deposited organic-rich marine sediments were likely reworked, thus returning the isotopically light carbon to the marine reservoir (Jarvis et al., 2002). Further evidence supporting the relationship between the sea-level drop and the lowering isotopic values comes from the characteristic surface in the isotopic profiles defining the lowest carbon values (< 2‰) and lowest oxygen values (approaching -6‰). This surface, recognized by a marked negative carbon and oxygen isotope excursion, coincides with the correlative conformity that represents the sequence boundary, and thus, with the lowest point of the relative sea level (Figs. 5 & 6). Furthermore, landwards, the sequence boundary is characterized by a subaerial unconformity, evidenced by truncation and paleokarst features, which further confirm the subaerial exposure of the platform (Bover-Arnal et al., 2009, 2022). This interpretation agrees with investigations in the NE margin of the Arabian plate that also demonstrated that erosional surfaces can be geochemically identified by characteristic negative isotope excursions (Rahimpour-Bonab et al., 2013; Mehrabi et al., 2022). Furthermore, comparable relationships between stable isotopes (mostly $\delta^{13}C$ values) and fluctuations in relative sea level have been also reported from the Oxfordian sedimentary record from central and southern Europe (Jenkyns, 1996), the Cenomanian-Turonian rocks from southern England (Jarvis et al., 2001), and the Campanian successions from northern Tunisia (Jarvis et al., 2002).

Significance of the carbonate geochemical imprints.---

It is remarkable that the timing and magnitude of the Aptian relative sea-level fall recorded in Depositional Sequence A align with the global sea-level event known as "KAp2" (Haq, 2014). This sea-level event is coeval with forced regressive wedges and deep incised valleys in the Tethys realm and in other Aptian carbonates worldwide (Rameil et al., 2012; Maurer et al., 2013; Horner et al., 2019). This lowering of relative sea level in the Tethys and elsewhere has been tentatively linked to glacio-eustasy (Dujoncquoy et al., 2018; Ray et al., 2019; Bover-Arnal et al., 2024), and thus, was likely triggered by changes in continental ice volume during an early Aptian cooling event (Stoll and Schrag, 1996; Hochuli et al., 1999; Steuber et al., 2005; Miller et al., 2005; Dujoncquoy et al., 2018; Davies et al., 2020). In the Galve Sub-basin, where the studied section is located, this cooling event has been reported from $\delta^{18}O$ values of well-preserved bivalves sampled along the Aptian succession (Fig. 1) (Bonin et al., 2016). Therefore, a discussion is presented next to explore if the reported isotope values in this study have paleoclimatic significance.

The isotopic trends discussed earlier in this section diverge from the typical isotopic patterns reported in studies linking paleoclimate and carbonate geochemistry (Bonin et al., 2016). In particular, sea-level drops caused by the formation of widespread continental ice sheets during climate cooling events are commonly interpreted from the correlation between sea-level regressions and positive $\delta^{18}O$ excursions (Stoll and Schrag, 2000; Pucéat et al., 2003; Steuber et al., 2022). This is because, during cooling periods, the lighter isotope (^{16}O) is readily taken by the glacial ice and the heavier isotope (^{18}O) is left behind, increasing the concentration of ^{18}O and the $\delta^{18}O$ value in the ocean (Kumar and Verma, 2021). In the current study, however, the

observed trend is contrary, and the forced regressive deposits record a negative $\delta^{18}O$ and $\delta^{13}C$ isotope excursion.

In paleoclimate studies, samples are commonly chosen to encompass homogeneous lithologies, generally mudstones, deposited in pelagic environments or in relatively deep-water settings. This selection aims to avoid isotopic modifications arising from relative sea-level fluctuations, subaerial exposures, and diagenesis (Stoll and Schrag, 2000; Vimpere et al., 2023). Alternatively, well-preserved foraminifers or other carbonate fossils that offer robust biostratigraphic constraints, are commonly used to extract paleoclimatic information (Pucéat et al., 2003; Bonin et al., 2016). In contrast to this, the stratigraphic interval analyzed here represents a well-preserved carbonate platform margin, where the carbonate facies, architecture, and likely the geochemical signature were mainly controlled by the relative sea-level fluctuations (Bover-Arnal et al., 2009, 2022; Gratacós et al., 2021). Because the shallow marine carbonates were exposed during the relative sea-level fall, the isotopic values of the regressive deposits are not interpreted as reflecting a climatic pattern (i.e., cooling event). Instead, they are interpreted to reflect the depositional environment and associated processes resulting from base-level fall during the subaerial exposure of the platform (Allan and Matthews, 1982) (Fig. 7).

In conclusion, our findings, which are in line with the interpreted third-order sea-level fall recorded in the Aptian carbonate platform studied, supports one of the previously debated sequence stratigraphic interpretations for the studied succession. Specifically, the basin floor wedge in the study area, interpreted by Bover-Arnal et al. (2009) as a forced regressive unit, was later reinterpreted as the upper part of a transgressive systems tract (Peropadre et al., 2013; Pomar and Haq, 2016; Pomar, 2020), with the latter authors arguing against evidence for a falling relative sea level during the deposition of this sedimentary wedge. However, our

carbonate geochemical data align with the interpreted exposure of the carbonate platform and thus, the relative sea-level drop proposed by Bover-Arnal et al. (2009). This interpretation is further corroborated by recent studies in the eastern Iberian Chain, where this major base-level fall was regionally recorded, either as forced regressive wedges or deep incised valley developed on highstand carbonate platforms (Gratacós et al., 2021; Bover-Arnal et al., 2022, 2024). According to our results, the high variation of C and O isotopic values recorded in the FRWST, together with the decreasing trend of values from the lower to the upper boundary of this unit, contrast with the relative homogeneous (and more positive) values characterizing the highstand deposits of both studied depositional sequences (Figs. 5 & 6). Therefore, we suggest that these contrasting geochemical patterns are the expression of different genetic types of deposits, which result from distinct stages of relative sea level (HST and FRWST, respectively). Moreover, a deeply incised subaerial unconformity (SU) located at the highstand platform top of Depositional Sequence A was correlated by Bover-Arnal et al. (2009) with the correlative conformity (CC) capping the forced regressive wedge (Fig. 2). The evidence of exposure in the SU, including local karst development, agrees with the geochemical signal of the CC displaying the lowest obtained C and O isotopic values. Thus, these observations are compatible with a sea-level regression.

Implications for linking sequence stratigraphy and carbonate geochemistry

In sequence stratigraphic interpretations, analyzing suitable outcrop analogs commonly furnishes detailed information below seismic resolution. This enables the recognition and characterization of stratal stacking patterns, facies architecture, and depositional systems (Catuneanu et al., 2009; Ruppel and Ward, 2013) as has been previously done in the studied Aptian section (Bover-Arnal et al., 2009, 2022). In subsurface reservoir studies for energy exploration, where the geological

interpretations and the scale of observations are required below the vertical seismic resolution, spatial and temporal discontinuities may compromise the resolution and the quality of the sequence stratigraphic interpretations (Carter et al., 1998). Accordingly, in cases where stratal patterns and their bounding surfaces are not well defined, the isotope records can serve as a complementary proxy to bridge specific data gaps in sequence stratigraphic analysis during the characterization of specific systems tracts and the subsequent reconstruction of relative sea-level changes.

In the study area, the geochemical data reveal that the isotope signatures recorded in the investigated Aptian platform carbonates were significantly influenced by depositional and environmental processes (such as changes in the origin of fluids) during fluctuations in relative sea level. The isotope trends reported here fall in line with the systems tracts and sequence-stratigraphic interpretation already defined by the evolution of facies and their stacking patterns (Figs. 6 & 7). Overall, despite the overlap of isotopic values displayed by different systems tracts, the forced regression and lowstand units display the widest range of $\delta^{13}C$ and $\delta^{18}O$ values obtained in this study, varying from around 0.0‰ to +4.0‰, and from -6.0‰ to -3.5‰, respectively. Despite the similar isotopic range, the FRWST can be recognized in the chemostratigraphic profiles by a general trend of decreasing $\delta^{13}C$ and $\delta^{18}O$ values from samples taken at the BSFR, which was formed when relative sea level was still high, to samples collected at the correlative conformity (SB), representing the lowest point of the relative sea level (Figs. 2, 5 & 6). By contrast, the LPWST shows an opposite pattern marked by a consistent increase in the $\delta^{13}C$ and a varying increase in the $\delta^{18}O$ values from samples close to the SB to samples collected at the TS. Thus, where the FRWST is preserved, the sequence boundary, which is represented by a subaerial unconformity that passes basinward to its marine correlative

conformity, and thus developed during the lowest point of relative sea level, correlates with a marked negative carbon and oxygen isotope excursion (Figs. 6 & 7). This likely suggests the progressive influence of the meteoric environment (and the exposure of the platform) during relative sea-level falling.

In contrast, the intervals of higher relative sea level (transgressive and highstand carbonate deposits) are geochemically recognized by a characteristic trend towards the highest $\delta^{13}C$ values documented in this study (>3.0‰) and the less varying (and less negative) $\delta^{18}O$ values (-5.5‰ to -3‰) registered throughout the succession investigated. This reflects, as discussed in the previous section, the maximum relative sea-level peak recorded in each depositional sequence and thus, the marine influence on the isotopic values.

Therefore, as proposed in this study, the application of isotope stratigraphy (i.e., chemostratigraphy) to carbonate rocks, within a sequence stratigraphic framework, enables the recognition of characteristic geochemical patterns in the vertical stratigraphic profile. In turn, these isotopic patterns linked to sequence stratigraphy might be correlatable among coeval carbonate successions from different geographical locations (Rahimpour-Bonab et al., 2013; Swart, 2015), enabling the determination of specific stages of relative sea level (systems tracts) within a poorly defined sequence stratigraphic framework.

Diagenetic and geochemical considerations for isotope stratigraphy

Diagenesis of marine carbonates commonly results in geochemical modifications of their original isotopic signature. With increasing burial depth, carbonate $\delta^{18}O$ values tend to decrease reflecting alteration of primary marine values under the influence of diagenetic fluids and increasing temperatures (Killingley, 1983). Therefore, using the geochemical data, this section

discusses if potential post-depositional effects could have compromised the stratigraphic significance of the measured isotope values. In particular, the $\delta^{13}C$ and $\delta^{18}O$ values measured in the studied Aptian succession show that, with only a few exceptions, bulk carbonates and separate carbonate components (matrix, grain, cement) from the same sample provided similar (or slightly varying) range of isotope values (Figs. 5 & 6). Thus, this could either indicate that the carbonate components are genetically related, that the isotope values were homogenized during carbonate deposition and early diagenesis, or that the original values were reset (overprinted) during later burial diagenesis (Swart et al., 2009; Swart, 2015). In this regard, characteristic geochemical patterns have been recognized in the vertical profile of the $\delta^{13}C$ and $\delta^{18}O$ values (Figs. 5 & 6). These geochemical profiles, as discussed in the previous section, define isotopic trends that broadly correlate with specific systems tracts. Therefore, although a certain extent of post-depositional modification of the isotope values cannot be disregarded, the geochemical trends of the studied platform carbonates have isotope stratigraphic significance considering that: (i) the isotopic values seem to vary according to the different systems tracts and their stratigraphic boundaries (Droxler et al., 1983; Roth and Reijmer, 2005); (ii) the overall observed trends, with positive carbon excursions matching rising sea levels and vice versa, follow the arguments and interpretations widely discussed in the literature (Föllmi et al., 1994; Vahrenkamp, 1996); and (iii) the different systems tracts, particularly the HST and TST from both depositional sequences, show little isotopic variation from the uppermost slope and towards the basin (as observed in LM samples, Fig. 5). Regarding this latter statement, if strong diagenesis had overprinted our isotopic values, HST and TST samples located respectively below and above the subaerial unconformity (SU), would have differing isotopic values likely resulting from meteoric vs marine diagenesis, respectively. Similarly, HST and TST samples

located near the uppermost slope (around the SU), would have different diagenetic overprint to HST and TST samples located around the correlative conformity (towards the basin), but again, we do not observe a different isotopic pattern that could indicate a strong diagenetic overprint. This also means that the TST and HST intervals display similar variation of C and O isotopic values, irrespective of the type of facies, which is an observation already made in modern carbonates from the Great Bahama Bank (Swart et al., 2009).

It is also noteworthy that the previous contributions linking geochemistry to sequence stratigraphy (Vahrenkamp, 1996; Jenkyns, 1996; Jarvis et al., 2001) have mainly used carbon isotope stratigraphy as a proxy for relative sea-level variation. This is because, in shallow marine carbonate settings, carbon isotopes tend to be rock-dominated (rather than fluid-dominated) and are less sensitive to temperature fractionation and diagenetic alteration compared to oxygen isotopes (Banner and Hanson, 1990; Marshall, 1992; Banner and Kaufman, 1994). This can explain, for instance, the greater scattering of the O isotope values in each systems tract with respect to the C isotope values in the same interval (Fig. 5). Nevertheless, the $\delta^{18}O$ values of carbonates are controlled not only by temperature but also by the $\delta^{18}O$ values of the formation (or diagenetic) fluids (because of the dominant oxygen reservoir of the fluids) (O'Neil et al., 1969; Muñoz-López et al., 2022; Cruset et al., 2023). In contrast to the negative $\delta^{18}O$ values of meteoric waters, for instance, marine fluids exhibit more positive values. Consequently, both isotope proxies ($\delta^{13}C$ and $\delta^{18}O$) in the studied platform carbonates serve as valuable tools for sequence stratigraphic analysis.

CONCLUSIONS

This study is an example of how isotope geochemistry and chemostratigraphy, when applied to ancient carbonate systems, may help in characterizing sequence-stratigraphic attributes. In the

studied Aptian platform carbonate succession, the $\delta^{18}O$ and $\delta^{13}C$ values show a strong correlation with a previously reported sequence stratigraphic framework. This allowed us to discriminate between divergent sequence stratigraphic interpretations previously proposed for the study area.

The systems tracts associated with relative sea-level highs (i.e., HST and TST) are characterized by a trend towards the highest $\delta^{13}C$ and $\delta^{18}O$ values obtained in this study, reaching up to +5.1‰ and up to -1.8‰, respectively. Among these, HST exhibits the most uniform values. In contrast, the systems tracts associated with stages of lower relative sea-level (i.e., FRWST and LPWST) show a greater isotope variability, with $\delta^{13}C$ values ranging from +0.5 to +4.5‰ and $\delta^{18}O$ values from -6.1 to -3.5‰. Within the FRWST, both isotope proxies progressively increase from the sequence boundary (SB) towards the BSFR, whereas in the LPWST, isotope values increase from the sequence boundary towards the TS. This implies that the lowest $\delta^{13}C$ and $\delta^{18}O$ values documented in this study are found at the SB (correlative conformity), coinciding with the lowest point of relative sea level. Furthermore, the results show that, with only a few exceptions, sampling bulk carbonates and separate carbonate components (micritic matrix, grain, cement) also yield similar isotope patterns.

The interpretations link carbonate isotope variations to a well-constrained sequence stratigraphic framework. These isotope variations are the expression of changing depositional and environmental processes during third-order Aptian sea-level fluctuations and can serve as analogue for: (i) carbonate platform successions characterized by poor (bio)stratigraphic resolution and weak to moderate diagenetic overprinting, and (ii) for potentially identifying and correlating systems tracts (specific stages of relative sea level) and their bounding surfaces in other locations.

ACKNOWLEDGEMENTS

This research was funded by the Startup Fund grant from the College of Petroleum Engineering and Geosciences to Khalid Al-Ramadan. We would like to thank CPG-KFUPM for the continuous support and access to its laboratory facilities. This paper is a contribution to IBERINSULA (PID2020-113912GB-I00). Research was partly funded by MCIN/AEI/10.13039/501100011033 and the European Regional Development Fund (ERDF), as well as by the Grup de Recerca Reconegut per la Generalitat de Catalunya 2021 SGR-Cat 00349 "Geologia Sedimentària". We sincerely thank the editor, the associate editor, and the two reviewers for their valuable feedback and efforts in helping us to enhance the quality of our research.

DATA AVAILABILITY STATEMENT

The data that support the findings of this study are available from the corresponding author upon reasonable request.

CONFLICT OF INTEREST

The authors declare that they have no known conflict of interest

CREDIT AUTHORSHIP CONTRIBUTION STATEMENT

D. Muñoz-López: Conceptualization, Data curation, Formal analysis, Investigation, Methodology, Validation, Visualization, Writing – original draft, Writing – review and editing. **A. Koeshidayatullah:** Conceptualization, Data curation, Formal analysis, Writing – review and editing. **T. Bover-Arnal:** Conceptualization, Formal analysis, Investigation, Writing – review and editing. **A. Herlambang:** Data curation, Methodology, Writing – review and editing. **J. D. Martín-Martín:** Investigation, Formal analysis, Writing – review and editing. **R. Salas:** Investigation, Formal analysis, Writing – review and editing. **J. D. Humphrey:** Funding

612 acquisition, Investigation, Writing – review and editing **K. Al-Ramadan:** Conceptualization,
613 Funding acquisition, Investigation, Writing – review and editing.

614 **REFERENCES**

615 ALLAN, J.R., and MATTHEWS, R.K., 1977, Carbon and oxygen isotopes as diagenetic and
616 stratigraphic tools: Surface and subsurface data, Barbados, West Indies: Geology, v. 5, p.
617 16.

618 ALLAN, J.R., and MATTHEWS, R.K., 1982, Isotope signatures associated with early meteoric
619 diagenesis: Sedimentology, v. 29, p. 797.

620 AL-RAMADAN, K., MORAD, S., PROUST, J.N., and AL-AASM, I., 2005, Distribution of Diagenetic
621 Alterations in Siliciclastic Shoreface Deposits within a Sequence Stratigraphic Framework:
622 Evidence from the Upper Jurassic, Boulonnais, NW France: Journal of Sedimentary
623 Research, v. 75, p. 943–959, doi: 10.2110/jsr.2005.072.

624 ANSELMETTI, F.S., EBERLI, G.P., and DING, Z.-D., 2000, From the Great Bahama Bank into the
625 Straits of Florida: A margin architecture controlled by sea-level fluctuations and ocean
626 currents: Geological Society of America Bulletin, v. 112, p. 829–844, doi: 10.1130/0016-
627 7606(2000)112<829:FTGBBI>2.0.CO;2.

628 BANNER, J.L., and HANSON, G.N., 1990, Calculation of simultaneous isotopic and trace element
629 variations during water-rock interaction with applications to carbonate diagenesis:
630 Geochimica et Cosmochimica Acta, v. 54, p. 3123–3137, doi: 10.1016/0016-
631 7037(90)90128-8.

BANNER, J.L., and KAUFMAN, J., 1994, The isotopic record of ocean chemistry and diagenesis preserved in non-luminescent brachiopods from Mississippian carbonate rocks, Illinois and Missouri: Geological Society of America Bulletin, v. 106, p. 1074–1082, doi: 10.1130/0016-7606(1994)106<1074:TIROOC>2.3.CO;2.

BONIN, A., PUCÉAT, E., VENNIN, E., MATTIOLI, E., AURELL, M., JOACHIMSKI, M., BARBARIN, N., and LAFFONT, R., 2016, Cool episode and platform demise in the Early Aptian: New insights on the links between climate and carbonate production: Paleoceanography, v. 31, p. 66–80, doi: 10.1002/2015PA002835.

BOVER-ARNAL, T., GUIMERÀ, J., MORENO-BEDMAR, J.A., FERRÀNDEZ-CAÑADELL, C., and SALAS, R., 2024, Aptian major changes in accommodation. New sedimentary evidence from the Maestrat Basin (E Iberia): Sedimentary Geology, v. 459, p. 106546, doi: 10.1016/j.sedgeo.2023.106546. https://linkinghub.elsevier.com/retrieve/pii/S003707382300218X.

BOVER-ARNAL, T., MORENO-BEDMAR, J.A., FRIJIA, G., PASCUAL-CEBRIAN, E., and SALAS, R., 2016, Chronostratigraphy of the Barremian – Early Albian of the Maestrat Basin (E Iberian Peninsula): integrating strontium-isotope stratigraphy and ammonoid biostratigraphy: Newsletters on Stratigraphy, v. 49, doi: 10.1127/nos/2016/0072. http://www.schweizerbart.de/papers/nos/detail/49/85408/Chronostratigraphy_of_the_Barremian__Early_Albian_?af=crossref.

BOVER-ARNAL, T., MORENO-BEDMAR, J.A., SALAS, R., SKELTON, P.W., BITZER, K., and GILI, E., 2010, Sedimentary evolution of an Aptian syn-rift carbonate system (Maestrat Basin, E

Spain): effects of accommodation and environmental change: Geologica Acta, v. 8, p. 249–280, doi: 10.1344/105.000001533.

BOVER-ARNAL, T., SALAS, R., GUIMERÀ, J., and MORENO-BEDMAR, J.A., 2022, Eustasy in the Aptian world: A vision from the eastern margin of the Iberian Plate: Global and Planetary Change, v. 214, p. 103849, doi: 10.1016/j.gloplacha.2022.103849.

BOVER-ARNAL, T., SALAS, R., MORENO-BEDMAR, J.A., and BITZER, K., 2009, Sequence stratigraphy and architecture of a late Early–Middle Aptian carbonate platform succession from the western Maestrat Basin (Iberian Chain, Spain): Sedimentary Geology, v. 219, p. 280–301, doi: 10.1016/j.sedgeo.2009.05.016.

BURLA, S., HEIMHOFER, U., HOCHULI, P.A., WEISSERT, H., and SKELTON, P., 2008, Changes in sedimentary patterns of coastal and deep-sea successions from the North Atlantic (Portugal) linked to Early Cretaceous environmental change: Palaeogeography, Palaeoclimatology, Palaeoecology, v. 257, p. 38–57, doi: 10.1016/j.palaeo.2007.09.010.

CANÉROT, J., CRESPO, A., and NAVARRO, D., 1979, Montalbán, hoja nº 518.Mapa Geológico de España 1:50.000. 2ª Serie. 1ª Edición. Servicio de Publicaciones, Ministerio de Industria y Energía, Madrid, 31 pp: .

CARTER, R.M., FULTHORPE, C.S., and NAISH, T.R., 1998, Sequence concepts at seismic and outcrop scale: the distinction between physical and conceptual stratigraphic surfaces: Sedimentary Geology, v. 122, p. 165–179, doi: 10.1016/S0037-0738(98)00104-3.

CATUNEANU, O., ABREU, V., BHATTACHARYA, J.P., BLUM, M.D., DALRYMPLE, R.W., ERIKSSON, P.G., FIELDING, C.R., FISHER, W.L., GALLOWAY, W.E., GIBLING, M.R., GILES, K.A., HOLBROOK, J.M., JORDAN, R., KENDALL, C.G.St.C., et al., 2009, Towards the

standardization of sequence stratigraphy: Earth-Science Reviews, v. 92, p. 1–33, doi: 10.1016/j.earscirev.2008.10.003.

CHRIST, N., IMMENHAUSER, A., AMOUR, F., MUTTI, M., TOMAS, S., AGAR, S.M., ALWAY, R., and KABIRI, L., 2012, Characterization and interpretation of discontinuity surfaces in a Jurassic ramp setting (High Atlas, Morocco): Sedimentology, v. 59, p. 249–290, doi: 10.1111/j.1365-3091.2011.01251.x.

CRUSET, D., VERGÉS, J., MUÑOZ-LÓPEZ, D., MORAGAS, M., CANTARERO, I., and TRAVÉ, A., 2023, Fluid evolution from extension to compression in the Pyrenean Fold Belt and Basque-Cantabrian Basin: A review: Earth-Science Reviews, v. 243, p. 104494, doi: 10.1016/j.earscirev.2023.104494.

D'ARGENIO, B., FERRERI, V., WEISSERT, H., AMODIO, S., BUONOCUNTO, F.P., and WISSLER, L., 2004, A multidisciplinary approach to global correlation and geochronology. The Cretaceous shallow-water carbonates of southern Appenines, Italy. In: D'Argenio, B., Fischer, A.G., Premoli Silva, I., Weissert, H., Ferreri, V. (Eds.), Cyclostratigraphy: Approaches and Case Histories. 81, pp. 103–122 SEPM, Spec. Publ.: Cyclostratigraphy: Approaches and Case Histories, doi: 10.2110/pec.04.81.0103.

D'AUTRY, W., WOLFS, K., YARRAMRAJU, S., SCHEPDAEL, A. Van, HOOGMARTENS, J., and ADAMS, E., 2010, Characterization and Improvement of Signal Drift Associated with Electron Ionization Quadrupole Mass Spectrometry: Analytical Chemistry, v. 82, p. 6480–6486, doi: 10.1021/ac100780s.

DAVIES, A., GRÉSELLE, B., HUNTER, S.J., BAINES, G., ROBSON, C., HAYWOOD, A.M., RAY, D.C., SIMMONS, M.D., and VAN BUCHEM, F.S.P., 2020, Assessing the impact of aquifer-eustasy

on short-term Cretaceous sea-level: Cretaceous Research, v. 112, p. 104445, doi: 10.1016/j.cretres.2020.104445.

DROXLER, A.W., SCHLAGER, W., and WHALLON, C.C., 1983, Quaternary aragonite cycles and oxygen-isotope record in Bahamian carbonate ooze: Geology, v. 11, p. 235–239.

DUJONCQUOY, E., GRÉLAUD, C., RAZIN, P., IMBERT, P., VAN BUCHEM, F., DUPONT, G., and LE BEC, A., 2018, Seismic stratigraphy of a Lower Cretaceous prograding carbonate platform (Oman) and implications for the eustatic sea-level curve: AAPG Bulletin, v. 102, p. 509–543, doi: 10.1306/04201715239.

EBERLI, G.P., 2000, The record of Neogene sea-level changes in the prograding carbonates along the Bahamas Transect—Leg 166 Synthesis, *in* Proceedings of the Ocean Drilling Program, 166 Scientific Results: Ocean Drilling Program.

EBERLI, G.P., ANSELMETTI, F.S., KROON, D., SATO, T., and WRIGHT, J.D., 2002, The chronostratigraphic significance of seismic reflections along the Bahamas Transect: Marine Geology, v. 185, p. 1–17, doi: 10.1016/S0025-3227(01)00287-0.

FÖLLMI, K.B., GODET, A., BODIN, S., and LINDER, P., 2006, Interactions between environmental change and shallow water carbonate buildup along the northern Tethyan margin and their impact on the Early Cretaceous carbon isotope record: Paleoceanography, v. 21 (4), doi: 10.1029/2006PA001313.

FÖLLMI, K.B., WEISSERT, H., BISPING, M., and FUNK, H., 1994, Phosphogenesis, carbon-isotope stratigraphy, and carbonate-platform evolution along the Lower Cretaceous northern Tethyan margin: Geological Society of America Bulletin, v. 106, p. 729–746, doi: 10.1130/0016-7606(1994)106<0729:PCISAC>2.3.CO;2.

GAUTIER, F., 1980, Villarluengo, hoja nº 543. Mapa Geológico de España 1:50.000. 2ª Serie. 1ª Edición. Servicio de Publicaciones, Ministerio de Industria y Energía, Madrid, 45 pp: .

GISCHLER, E., SWART, P.K., and LOMANDO, A.J., 2009, Stable Isotopes of Carbon and Oxygen in Modern Sediments of Carbonate Platforms, Barrier Reefs, Atolls and Ramps: Patterns and Implications, *in* Perspectives in Carbonate Geology: Wiley, p. 61–74.

GRATACÓS, Ò., BOVER-ARNAL, T., CLAVERA-GISPERT, R., CARMONA, A., and GARCÍA-SELLÉS, D., 2021, Forward numerical modelling constraining environmental parameters (Aptian carbonate system, E Iberia): Marine and Petroleum Geology, v. 124, p. 104822, doi: 10.1016/j.marpetgeo.2020.104822.

GRÖCKE, D.R., HESSELBO, S.P., and JENKYNS, H.C., 1999, Carbon-isotope composition of Lower Cretaceous fossil wood: Ocean-atmosphere chemistry and relation to sea-level change: Geology, v. 27, p. 155, doi: 10.1130/0091-7613(1999)027<0155:CICOLC>2.3.CO;2.

GUIMERÀ, J., MAS, R., and ALONSO, A., 2004, Intraplate deformation in the NW Iberian Chain: Mesozoic extension and Tertiary contractional inversion: Journal of the Geological Society, v. 161, p. 291–303, doi: 10.1144/0016-764903-055.

HAQ, B.U., 2014, Cretaceous eustasy revisited: Global and Planetary Change, v. 113, p. 44–58, doi: 10.1016/j.gloplacha.2013.12.007.

HAQ, B.U., HARDENBOL, J., and VAIL, P.R., 1987, Chronology of Fluctuating Sea Levels Since the Triassic: Science, v. 235, p. 1156–1167, doi: 10.1126/science.235.4793.1156.

739 HARRIS, P.M., and SALLER, A.H., 1999, Subsurface expression of the Capitan depositional
740 system and implications for hydrocarbon reservoirs, northeastern Delaware basin, in A.H.
741 Saller, P.M. Harris, B. Kirkland, and S. Mazzullo, eds., Geologic Framework of the Capitan
742 Reef: SEPM (Society for Sedimentary Geology) Special Publication 65, p. 37-49: Geologic
743 Framework of the Capitan Reef, v. 65, doi: 10.2110/pec.99.65.0037.

744 HOCHULI, P.A., MENEGATTI, A.P., WEISSERT, H., RIVA, A., ERBA, E., and SILVA, I.P., 1999,
745 Episodes of high productivity and cooling in the early Aptian Alpine Tethys: Geology, v.
746 27, p. 657, doi: 10.1130/0091-7613(1999)027<0657:EOHPAC>2.3.CO;2.

747 HORNER, S.C., HUBBARD, S.M., MARTIN, H.K., HAGSTROM, C.A., and LECKIE, D.A., 2019, The
748 impact of Aptian glacio-eustasy on the stratigraphic architecture of the Athabasca Oil
749 Sands, Alberta, Canada: Sedimentology, v. 66, p. 1600–1642, doi: 10.1111/sed.12545.

750 HUNT, D., and TUCKER, M.E., 1992, Stranded parasequences and the forced regressive wedge
751 systems tract: deposition during base-level'fall: Sedimentary Geology, v. 81, p. 1–9, doi:
752 10.1016/0037-0738(92)90052-S.

753 IMMENHAUSER, A., KENTER, J.A.M., GANSSEN, G., BAHAMONDE, J.R., VAN VLIET, A., and
754 SAHER, M.H., 2002, Origin and Significance of Isotope Shifts in Pennsylvanian Carbonates
755 (Asturias, NW Spain): Journal of Sedimentary Research, v. 72, p. 82–94, doi:
756 10.1306/051701720082.

757 IMMENHAUSER, A., DELLA PORTA, G., KENTER, J.A.M., and BAHAMONDE, J.R., 2003, An
758 alternative model for positive shifts in shallow-marine carbonate $\delta^{13}C$ and $\delta^{18}O$:
759 Sedimentology, v. 50, p. 953–959, doi: 10.1046/j.1365-3091.2003.00590.x.
760 https://onlinelibrary.wiley.com/doi/10.1046/j.1365-3091.2003.00590.x.

JARVIS, I., MABROUK, A., MOODY, R.T.J., and DE CABRERA, S., 2002, Late Cretaceous (Campanian) carbon isotope events, sea-level change and correlation of the Tethyan and Boreal realms: Palaeogeography, Palaeoclimatology, Palaeoecology, v. 188, p. 215–248, doi: 10.1016/S0031-0182(02)00578-3.

JARVIS, I., MURPHY, A.M., and GALE, A.S., 2001, Geochemistry of pelagic and hemipelagic carbonates: criteria for identifying systems tracts and sea-level change: Journal of the Geological Society, v. 158, p. 685–696, doi: 10.1144/jgs.158.4.685.

JENKYNS, H.C., 1996, Relative sea-level change and carbon isotopes: data from the Upper Jurassic (Oxfordian) of central and Southern Europe: Terra Nova, v. 8, p. 75–85, doi: 10.1111/j.1365-3121.1996.tb00727.x.

KILLINGLEY, J.S., 1983, Effects of diagenetic recrystallization on 18O/16O values of deep-sea sediments: Nature, v. 301, p. 594–597.

KRULL, E.S., LEHRMANN, D.J., DRUKE, D., KESSEL, B., YU, Y., and LI, R., 2004, Stable carbon isotope stratigraphy across the Permian–Triassic boundary in shallow marine carbonate platforms, Nanpanjiang Basin, south China: Palaeogeography, Palaeoclimatology, Palaeoecology, v. 204, p. 297–315, doi: 10.1016/S0031-0182(03)00732-6.

KUMAR, V., and VERMA, K., 2021, Geological records of climate change, *in* Global Climate Change: Elsevier, p. 175–185.

LIESA, C.L., SORIA, A.R., MELÉNDEZ, N., and MELÉNDEZ, A., 2006, Extensional fault control on the sedimentation patterns in a continental rift basin: El Castellar Formation, Galve sub-basin, Spain: Journal of the Geological Society, v. 163, p. 487–498, doi: 10.1144/0016-764904-169.

MAGARITZ, M., 1989, 13C minima follow extinction events: A clue to faunal radiation: Geology, v. 17, p. 337, doi: 10.1130/0091-7613(1989)017<0337:CMFEEA>2.3.CO;2.

MARSHALL, J.D., 1992, Climatic and oceanographic isotopic signals from the carbonate rock record and their preservation: Geological Magazine, v. 129, p. 143–160, doi: 10.1017/S0016756800008244.

MARTÍN-CHIVELET, J., LÓPEZ-GÓMEZ, J., AGUADO, R., A.C., ARRIBAS, J., ARRIBAS, M.E., AURELL, M., BÁDENAS, B., BENITO, M.I., BOVER-ARNAL, T., CASAS-SAINZ, A., CASTRO, J.M., CORUÑA, F., DE GEA, G.A., FORNÓS, J.J., et al., 2019, The late Jurassic–early cretaceous rifting. In: Quesada, C., Oliveira, J.T. (Eds.), The Geology of Iberia: A Geodynamic Approach. Volume 3: The Alpine Cycle: Springer, Heidelberg, pp. 60–63.

MAURER, F., VAN BUCHEM, F.S.P., EBERLI, G.P., PIERSON, B.J., RAVEN, M.J., LARSEN, P.-H., AL-HUSSEINI, M.I., and VINCENT, B., 2013, Late Aptian long-lived glacio-eustatic lowstand recorded on the Arabian Plate: Terra Nova, v. 25, p. 87–94, doi: 10.1111/ter.12009.

MEHRABI, H., NAVIDTALAB, A., RAHIMPOUR-BONAB, H., and HEIMHOFER, U., 2022, Geochemical expression of sequence stratigraphic surfaces: A case from Upper Cretaceous shallow-water carbonates of southeastern Neo-Tethys margin, SW Iran: Cretaceous Research, v. 140, p. 105329, doi: 10.1016/j.cretres.2022.105329.

MILLER, K.G., KOMINZ, M.A., BROWNING, J. V., WRIGHT, J.D., MOUNTAIN, G.S., KATZ, M.E., SUGARMAN, P.J., CRAMER, B.S., CHRISTIE-BLICK, N., and PEKAR, S.F., 2005, The Phanerozoic Record of Global Sea-Level Change: Science, v. 310, p. 1293–1298, doi: 10.1126/science.1116412.

MORAD, S., AL-RAMADAN, K., KETZER, J.M., and DE ROS, L.F., 2010, The impact of diagenesis on the heterogeneity of sandstone reservoirs: A review of the role of depositional facies and sequence stratigraphy: AAPG Bulletin, v. 94, p. 1267–1309, doi: 10.1306/04211009178.

MORAD, S., KETZER, J.M., and DE ROS, L.F., 2013, Linking Diagenesis to Sequence Stratigraphy: An Integrated Toolfor Understanding and Predicting Reservoir Quality Distribution, *in* Morad, S., Ketzer, J.M., and De Ros, L.F., eds., Linking Diagenesis to Sequence Stratigraphy: Wiley, p. 1–36. https://onlinelibrary.wiley.com/doi/10.1002/9781118485347.ch1.

MORAD, S., KETZER, J.M., and DE ROS, L.F., 2000, Spatial and temporal distribution of diagenetic alterations in siliciclastic rocks: implications for mass transfer in sedimentary basins: Sedimentology, v. 47, p. 95–120, doi: 10.1046/j.1365-3091.2000.00007.x.

MORENO-BEDMAR, J.A., COMPANY, M., BOVER-ARNAL, T., SALAS, R., DELANOY, G., MAURRASSE, Florentin.J.-M.R., GRAUGÉS, A., and MARTINEZ, R., 2010, Lower Aptian ammonite biostratigraphy in the Maestrat Basin (Eastern Iberian Chain, Eastern Spain). A Tethyan transgressive record enhanced by synrift subsidence: Geologica Acta, v. 8, p. 281–299.

MUÑOZ-LÓPEZ, D., CRUSET, D., VERGÉS, J., CANTARERO, I., BENEDICTO, A., MANGENOT, X., ALBERT, R., GERDES, A., BERANOAGUIRRE, A., and TRAVÉ, A., 2022, Spatio-temporal variation of fluid flow behavior along a fold: The Bóixols-Sant Corneli anticline (Southern Pyrenees) from U–Pb dating and structural, petrographic and geochemical constraints: Marine and Petroleum Geology, v. 143, p. 105788, doi: 10.1016/j.marpetgeo.2022.105788.

MURRAY, S.T., HIGGINS, J.A., HOLMDEN, C., LU, C., and SWART, P.K., 2021, Geochemical fingerprints of dolomitization in Bahamian carbonates: Evidence from sulphur, calcium, magnesium and clumped isotopes: Sedimentology, v. 68, p. 1–29, doi: 10.1111/sed.12775.

MURRAY, S.T., and SWART, P.K., 2017, Evaluating formation fluid models and calibrations using clumped isotope paleothermometry on Bahamian dolomites: Geochimica et Cosmochimica Acta, v. 206, p. 73–93, doi: 10.1016/j.gca.2017.02.021.

O'NEIL, J.R., CLAYTON, R.N., and MAYEDA, T.K., 1969, Oxygen Isotope Fractionation in Divalent Metal Carbonates: The Journal of Chemical Physics, v. 51, p. 5547–5558, doi: 10.1063/1.1671982. https://pubs.aip.org/jcp/article/51/12/5547/85541/Oxygen-Isotope-Fractionation-in-Divalent-Metal.

PEROPADRE, C., LIESA, C.L., and MELÉNDEZ, N., 2013, High-frequency, moderate to high-amplitude sea-level oscillations during the late Early Aptian: Insights into the Mid-Aptian event (Galve sub-basin, Spain): Sedimentary Geology, v. 294, p. 233–250, doi: 10.1016/j.sedgeo.2013.05.019.

POMAR, L., 2020, Carbonate systems, *in* Regional Geology and Tectonics: Principles of Geologic Analysis: Elsevier, p. 235–311.

POMAR, L., GILI, E., OBRADOR, A., and WARD, W.C., 2005, Facies architecture and high-resolution sequence stratigraphy of an Upper Cretaceous platform margin succession, southern central Pyrenees, Spain: Sedimentary Geology, v. 175, p. 339–365, doi: 10.1016/j.sedgeo.2004.11.009.

POMAR, L., and HAQ, B.U., 2016, Decoding depositional sequences in carbonate systems: Concepts vs experience: Global and Planetary Change, v. 146, p. 190–225, doi: 10.1016/j.gloplacha.2016.10.001.

POPP, B.N., PODOSEK, F.A., BRANNON, J.C., ANDERSON, T.F., and PIER, J., 1986, 87Sr/86Sr ratios in Permo-Carboniferous sea water from the analyses of well-preserved brachiopod shells: Geochimica et Cosmochimica Acta, v. 50, p. 1321–1328, doi: 10.1016/0016-7037(86)90308-X. https://linkinghub.elsevier.com/retrieve/pii/001670378690308X.

POSAMENTIER, H.W., ALLEN, G.P., JAMES, D.P., and TESSON, M., 1992, Forced Regressions in a Sequence Stratigraphic Framework: Concepts, Examples, and Exploration Significance: AAPG Bulletin, v. 76, doi: 10.1306/BDFF8AA6-1718-11D7-8645000102C1865D. http://search.datapages.com/data/doi/10.1306/BDFF8AA6-1718-11D7-8645000102C1865D.

PUCÉAT, E., LÉCUYER, C., SHEPPARD, S.M.F., DROMART, G., REBOULET, S., and GRANDJEAN, P., 2003, Thermal evolution of Cretaceous Tethyan marine waters inferred from oxygen isotope composition of fish tooth enamels: Paleoceanography, v. 18, doi: 10.1029/2002PA000823.

RAHIMPOUR-BONAB, H., MEHRABI, H., NAVIDTALAB, A., OMIDVAR, M., ENAYATI-BIDGOLI, A.H., SONEI, R., SAJJADI, F., AMIRI-BAKHTYAR, H., ARZANI, N., and IZADI-MAZIDI, E., 2013, Paleo-exposure surfaces in Cenomanian – Santonian Carbonate Reservoirs in the Dezful Embayment, SW Iran: Journal of Petroleum Geology, v. 36, p. 335–362, doi: 10.1111/jpg.12560.

RAMEIL, N., IMMENHAUSER, A., CSOMA, A.É., and WARRLICH, G., 2012, Surfaces with a long history: the Aptian top Shu'aiba Formation unconformity, Sultanate of Oman: Sedimentology, v. 59, p. 212–248, doi: 10.1111/j.1365-3091.2011.01279.x.

RAY, D.C., VAN BUCHEM, F.S.P., BAINES, G., DAVIES, A., GRÉSELLE, B., SIMMONS, M.D., and ROBSON, C., 2019, The magnitude and cause of short-term eustatic Cretaceous sea-level change: A synthesis: Earth-Science Reviews, v. 197, p. 102901, doi: 10.1016/j.earscirev.2019.102901.

REIJMER, J.J.G., SWART, P.K., BAUCH, T., OTTO, R., REUNING, L., ROTH, S., and ZECHEL, S., 2009, A Re-Evaluation of Facies on Great Bahama Bank I: New Facies Maps of Western Great Bahama Bank, *in* Perspectives in Carbonate Geology: Wiley, p. 29–46.

REUNING, L., REIJMER, J.J.G., BETZLER, C., TIMMERMANN, A., and STEPH, S., 2006, Sub-Milankovitch cycles in periplatform carbonates from the early Pliocene Great Bahama Bank: Paleoceanography, v. 21, doi: 10.1029/2004PA001075.

ROTH, S., and REIJMER, J.J.G., 2005, Holocene millennial to centennial carbonate cyclicity recorded in slope sediments of the Great Bahama Bank and its climatic implications: Sedimentology, v. 52, p. 161–181, doi: 10.1111/j.1365-3091.2004.00684.x.

RUPPEL, S.C., and WARD, W.B., 2013, Outcrop-based characterization of the Leonardian carbonate platform in west Texas: Implications for sequence-stratigraphic styles in the Lower Permian: AAPG Bulletin, v. 97, p. 223–250, doi: 10.1306/05311212013.

SALAS, R., and CASAS, A., 1993, Mesozoic extensional tectonics, stratigraphy and crustal evolution during the Alpine cycle of the eastern Iberian basin: Tectonophysics, v. 228, p. 33–55, doi: 10.1016/0040-1951(93)90213-4.

SALAS, R., GUIMERÀ, J., MAS, R., MARTÍN-CLOSAS, C., MELÈNDEZ, A., and ALONSO, A., 2001, Evolution of the Mesozoic Central Iberian Rift System and its Cainozoic inversion (Iberian Chain). In: Ziegler, P.A., Cavazza, W., Roberston, A.H.F., Crasquin-Soleau, S. (Eds.), Peri-Tethys Memoir 6: Peri-Tethyan Rift/Wrench Basins and Passive Margins, 186: Mémoires du Muséum National d'Histoire Naturelle, Paris, pp. 145–186.

SALTZMAN, M.R., 2002, Carbon and oxygen isotope stratigraphy of the Lower Mississippian (Kinderhookian–lower Osagean), western United States: Implications for seawater chemistry and glaciation: Geological Society of America Bulletin, v. 114, p. 96–108, doi: 10.1130/0016-7606(2002)114<0096:CAOISO>2.0.CO;2.

SALTZMAN, M.R., 2003, Late Paleozoic ice age: Oceanic gateway or pCO2? Geology, v. 31, p. 151, doi: 10.1130/0091-7613(2003)031<0151:LPIAOG>2.0.CO;2.

SATTLER, U., IMMENHAUSER, A., HILLGARTNER, H., and ESTEBAN, M., 2005, Characterization, lateral variability and lateral extent of discontinuity surfaces on a Carbonate Platform (Barremian to Lower Aptian, Oman): Sedimentology, v. 52, p. 339–361, doi: 10.1111/j.1365-3091.2005.00701.x.

SCHLAGER, W., 2005, Fundamentals of sequence stratigraphy, *in* Carbonate Sedimentology and Sequence Stratigraphy: SEPM (Society for Sedimentary Geology), p. 83–104. https://pubs.geoscienceworld.org/books/book/1068/chapter/10545655/.

SPEZZAFERRI, S., MCKENZIE, J.A., and ISERN, A., 2002, Linking the oxygen isotope record of late Neogene eustasy to sequence stratigraphic patterns along the Bahamas margin: results from a paleoceanographic study of ODP Leg 166, Site 1006 sediments: Marine Geology, v. 185, p. 95–120, doi: 10.1016/S0025-3227(01)00292-4.

910 STEUBER, T., ALSUWAIDI, M., HENNHOEFER, D., SULIEMAN, H., ALBLOOSHI, A., MCALPIN,
911 T.D., and SHEBL, H., 2022, Environmental change and carbon-cycle dynamics during the
912 onset of Cretaceous oceanic anoxic event 1a from a carbonate-ramp depositional system,
913 Abu Dhabi, U.A.E.: Palaeogeography, Palaeoclimatology, Palaeoecology, v. 601, p.
914 111086, doi: 10.1016/j.palaeo.2022.111086.

915 STEUBER, T., RAUCH, M., MASSE, J.-P., GRAAF, J., and MALKOČ, M., 2005, Low-latitude
916 seasonality of Cretaceous temperatures in warm and cold episodes: Nature, v. 437, p. 1341–
917 1344, doi: 10.1038/nature04096.

918 STOLL, H.M., and SCHRAG, D.P., 1996, Evidence for Glacial Control of Rapid Sea Level
919 Changes in the Early Cretaceous: Science, v. 272, p. 1771–1774, doi:
920 10.1126/science.272.5269.1771.

921 STOLL, H.M., and SCHRAG, D.P., 2000, High-resolution stable isotope records from the Upper
922 Cretaceous rocks of Italy and Spain: Glacial episodes in a greenhouse planet? Geological
923 Society of America Bulletin, v. 112, p. 308–319, doi: 10.1130/0016-
924 7606(2000)112<0308:HRSIRF>2.3.CO;2.

925 SWART, P.K., 2015, The geochemistry of carbonate diagenesis: The past, present and future:
926 Sedimentology, v. 62, p. 1233–1304, doi: 10.1111/sed.12205.

927 SWART, P.K., and EBERLI, G., 2005, The nature of the δ13C of periplatform sediments:
928 Implications for stratigraphy and the global carbon cycle: Sedimentary Geology, v. 175, p.
929 115–129, doi: 10.1016/j.sedgeo.2004.12.029.

930 SWART, P.K., REIJMER, J.J.G., and OTTO, R., 2009, A Re-Evaluation of Facies on Great Bahama
931 Bank II: Variations in the δ ^{13} C, δ ^{18} O and Mineralogy of Surface Sediments, *in*
932 Perspectives in Carbonate Geology: Wiley, p. 47–59.

933 TUCKER, M.E., 1993, Carbonate Diagenesis and Sequence Stratigraphy, *in* Sedimentology
934 Review/1: Wiley, p. 51–72.
935 https://onlinelibrary.wiley.com/doi/10.1002/9781444304534.ch4.

936 VAHRENKAMP, V.C., 1996, Carbon Isotope Stratigraphy of the Upper Kharaib and Shuaiba
937 Formations: Implications for the Early Cretaceous Evolution of the Arabian Gulf Region:
938 AAPG Bulletin, v. 80, doi: 10.1306/64ED8868-1724-11D7-8645000102C1865D.

939 VAIL, P.R., AUDEMARD, F., BOWMAN, S.A., EISNER, P.N., and PEREZ-CRUZ, C., 1991, The
940 stratigraphic signatures of tectonics, eustasy and sedimentology - an overview. In: Einsele,
941 G., Ricken, W., Seilacher, A. (Eds.), Cycles and Events in Stratigraphy: Springer, Berlin,
942 pp. 617–659.

943 VEIZER, J., ALA, D., AZMY, K., BRUCKSCHEN, P., BUHL, D., BRUHN, F., GARDEN, G.A.F.,
944 DIENER, A., EBNETH, S., GODDERIS, Y., JASPER, T., KORTE, C., PAWELLEK, F., PODLAHA,
945 O.G., et al., 1999, 87Sr/86Sr, δ13C and δ18O evolution of Phanerozoic seawater: Chemical
946 Geology, v. 161, p. 59–88, doi: 10.1016/S0009-2541(99)00081-9.
947 http://dx.doi.org/10.1016/S0009-2541(99)00081-9.

948 VIMPERE, L., SPANGENBERG, J.E., ROIGE, M., ADATTE, T., DE KAENEL, E., FILDANI, A., CLARK,
949 J., SAHOO, S., BOWMAN, A., STERNAI, P., and CASTELLTORT, S., 2023, Carbon isotope and
950 biostratigraphic evidence for an expanded Paleocene–Eocene Thermal Maximum

sedimentary record in the deep Gulf of Mexico: Geology, v. 51, p. 334–339, doi: 10.1130/G50641.1.

WEISSERT, H., LINI, A., FÖLLMI, K.B., and KUHN, O., 1998, Correlation of Early Cretaceous carbon isotope stratigraphy and platform drowning events: a possible link? Palaeogeography, Palaeoclimatology, Palaeoecology, v. 137, p. 189–203, doi: 10.1016/S0031-0182(97)00109-0.

FIGURE CAPTIONS

Fig. 1. From right to left: simplified structural and isopach map of the Maestrat Basin (located in the eastern Iberian Chain, eastern Iberian Peninsula) during the Late Jurassic-Early Cretaceous rifting, and geological map of the central Galve Sub-basin. The schematic transect A-A' is found in Fig. 2A and the red start indicates the location of the study area at Las Mingachas section. The geological map was modified from Canérot et al. (1979), Gautier (1980) and Bover-Arnal et al. (2022), whereas the structural map of the Maestrat Basin was modified from Salas et al. in Martín-Chivelet et al. (2019) and Bover-Arnal et al. (2022).

Fig. 2. Sequence stratigraphic framework of Las Mingachas section. (A) Simplified and schematic cross section showing the platform to basin transition setting cropping out in the study area. See Fig. 1 for the location of the section A-A'. The dashed red square represents the panoramic photo showed in Figs. B and C. (B) Panoramic view and (C) sequence stratigraphic interpretation of Las Mingachas. The grey bar represents the location of the stratigraphic log

(Fig. 3). The stages of relative sea-level fluctuation are also included. Modified from Bover-Arnal *et al.* (2009, 2022).

Fig. 3. Location of samples in outcrop (upper) and in the stratigraphic log of the studied Aptian sedimentary succession (lower). The stratigraphic log shows the chronostratigraphic and sequence stratigraphic analysis. Ammonite data come from Moreno-Bedmar et al. (2010) and Bover-Arnal et al. (2016). Samples were collected considering two sampling strategies for comparison. LM samples (LM1-LM18) covers laterally the full studied outcrop, whereas vertical log samples (samples 131-174) runs parallel to the stratigraphic log. Colored dots link the samples to the specific stages of the relative sea-level curve (systems tracts).

Fig. 4. (A) Outcrop image showing the location of representative samples where the sedimentary facies of the section were logged and sampled. (B) Wackestone to packstone limestones of the upper part of the Forcall Formation showing *Palorbitolina lenticularis* (P) (HST, Depositional Sequence A). (C) Forced regressive deposits of the Villarroya de los Pinares Formation characterized by a grainstone texture with specimens of *Orbitolinopsis* (O) (FRWST, Depositional Sequence A). (D) Lowstand deposits of the Villarroya de los Pinares Formation exhibiting a rudstone texture with sections of corals and calcareous algae (LPWST, Depositional Sequence B). (E) Transgressive limestones of the Villarroya de los Pinares Formation showing a rudstone texture with fragments of rudist shells, corals and calcareous algae (TST, Depositional Sequence B).

Fig. 5. Stratigraphic log of the Aptian sedimentary succession studied at Las Mingachas including the sequence stratigraphic analysis and the carbon and oxygen isotope profiles measured. LM samples include bulk and separate carbonate components, whereas vertical log samples consist of bulk carbonates. Legend of symbols referring to sedimentary structures and sample numbers and references are explained in Fig. 3.

Fig. 6. (A) Crossplot showing the $\delta^{18}O$ vs $\delta^{13}C$ values of the studied platform carbonate succession. The colored box indicates the typical isotope values of Lower Cretaceous marine carbonates. (B) Evolution of $\delta^{13}C$ values through time linked to the depositional sequences and the corresponding systems tract. The $\delta^{13}C$ profile is characterized by an episode of lowermost C values separating two intervals of more positive C values. The red boxes represent isotope values from the closest samples to the sequence boundary, which coincide with the lowermost C and O isotopic values.

Fig. 7. Schematic diagram showing the interpreted relationship among relative sea-level fluctuations, sedimentation, sequence stratigraphic analysis, and the observed geochemical patterns of the studied Aptian platform carbonates. Note that the specific stages of relative sea-level high (coinciding with highstand and transgressive system tracts) show a general trend towards more positive and less negative $\delta^{13}C$ and $\delta^{18}O$ values, respectively. In contrast, the stages of lower relative sea level (forced regressive and lowstand system tracts) yield less positive $\delta^{13}C$ and $\delta^{18}O$ values. The correlative conformity representing the sequence boundary is marked by a negative C and O isotopic excursion.

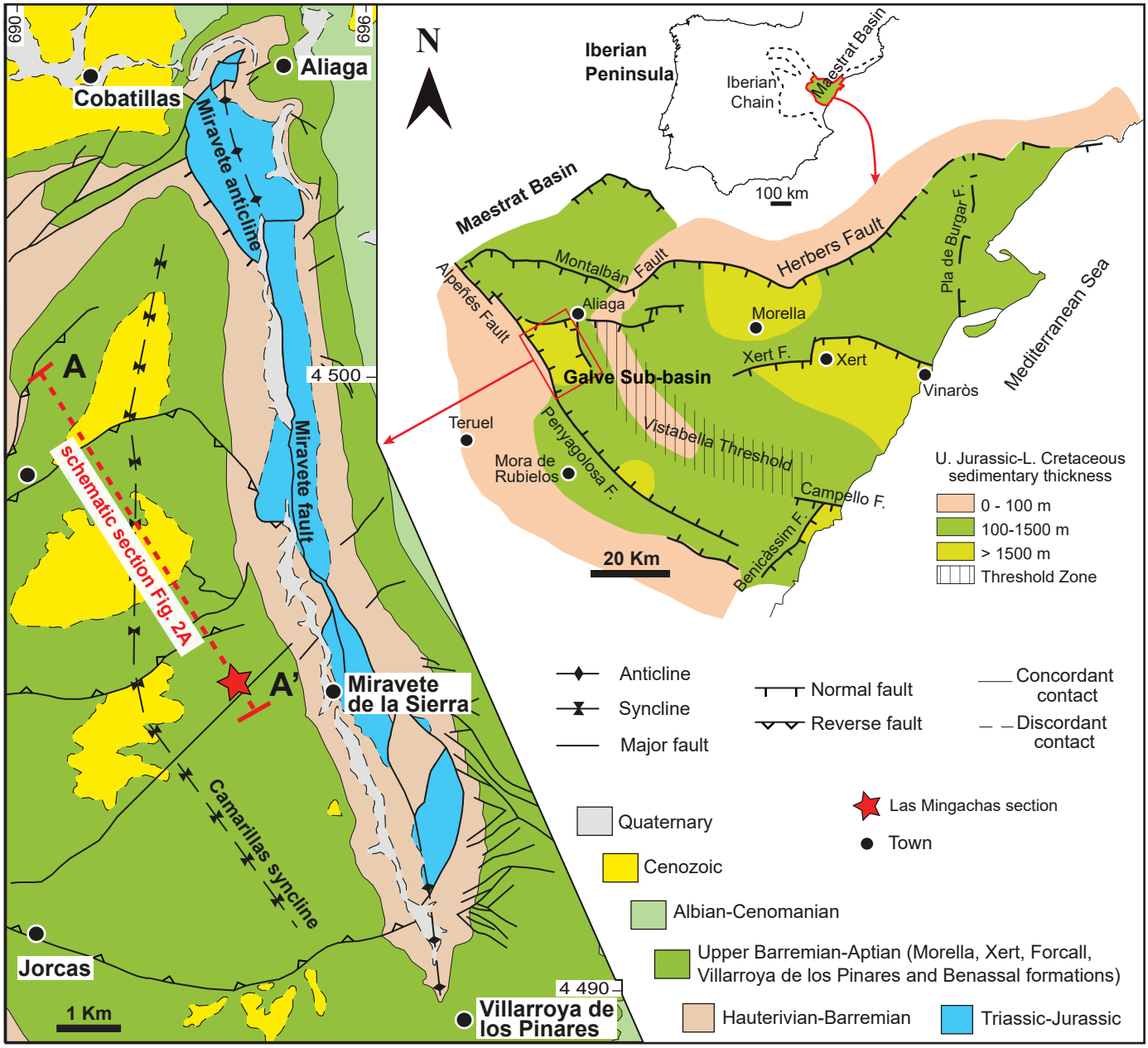

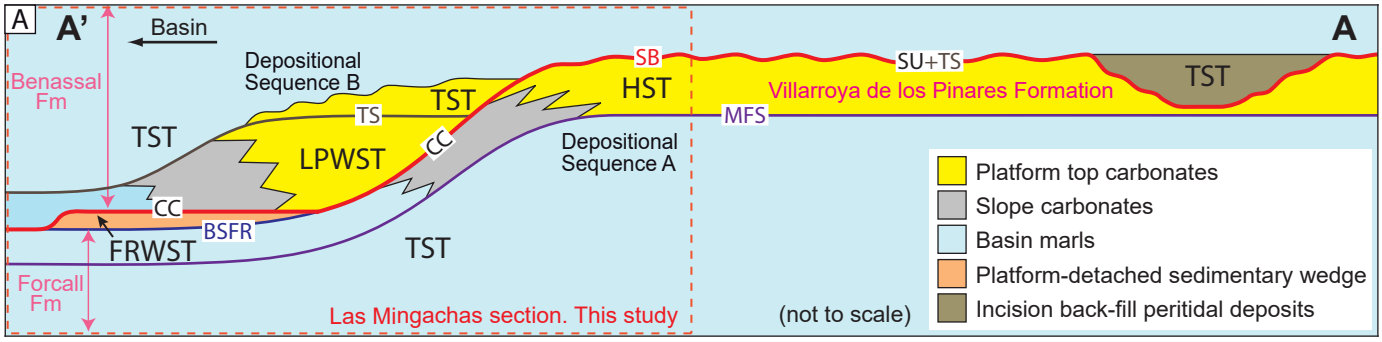

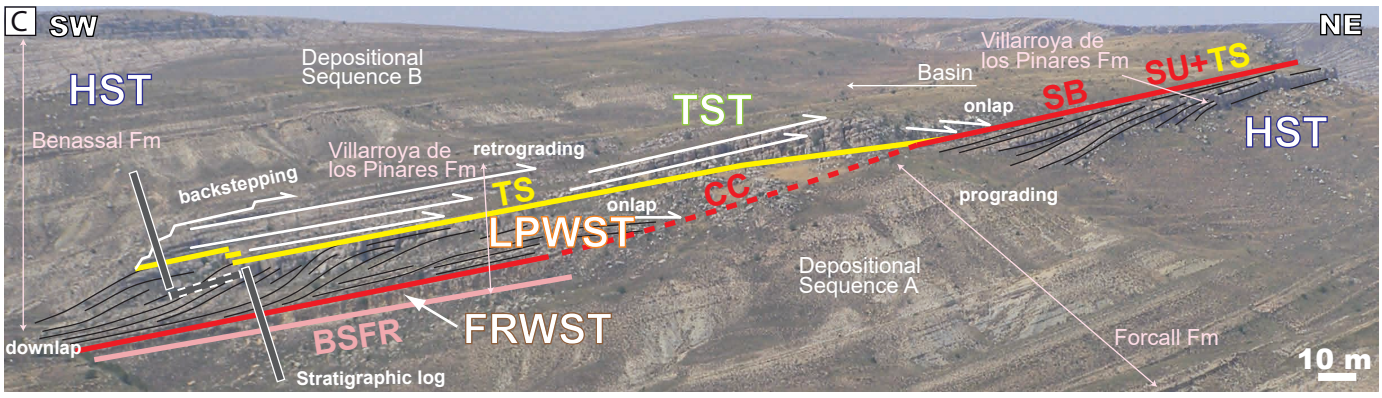

Key

HST: Highstand Systems Tract

FRWST: Forced Regressive Wedge Systems Tract

LPWST: Lowstand Prograding Wedge Systems Tract

TST: Transgressive Systems Tract

BSFR: Basal Surface of Forced Regression

SB: Sequence Boundary

TS: Transgressive Surface

MFS: Maximum Flooding Surface

CC: Correlative Conformity

SU: Subaerial Unconformity

Relative sea-level fluctuation

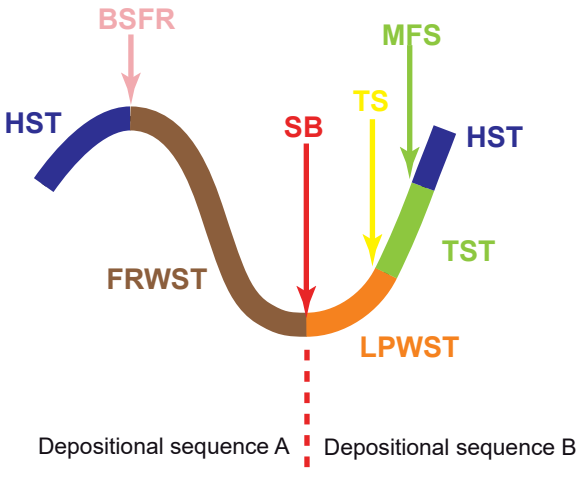

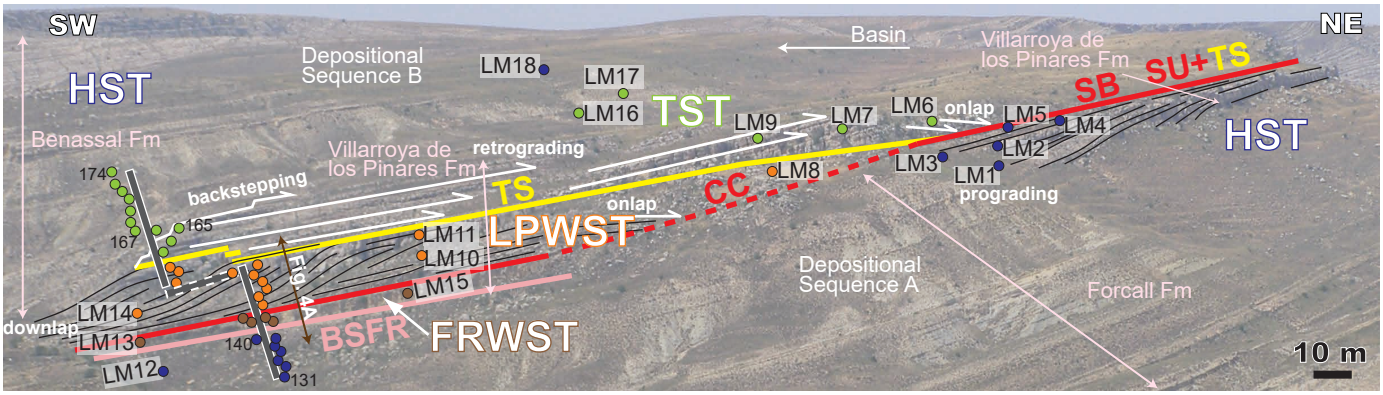

Stratigraphic log and vertical log samples

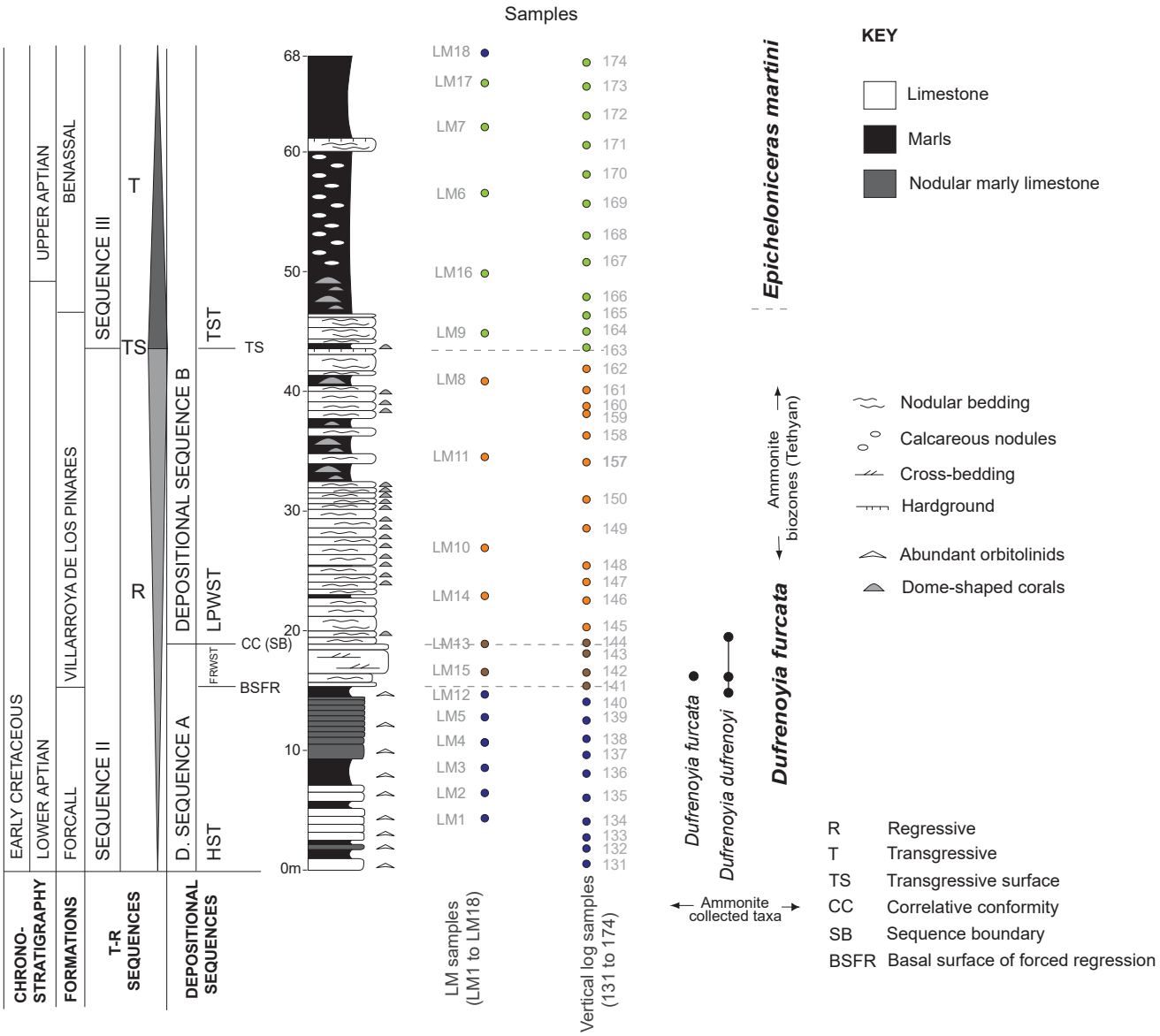

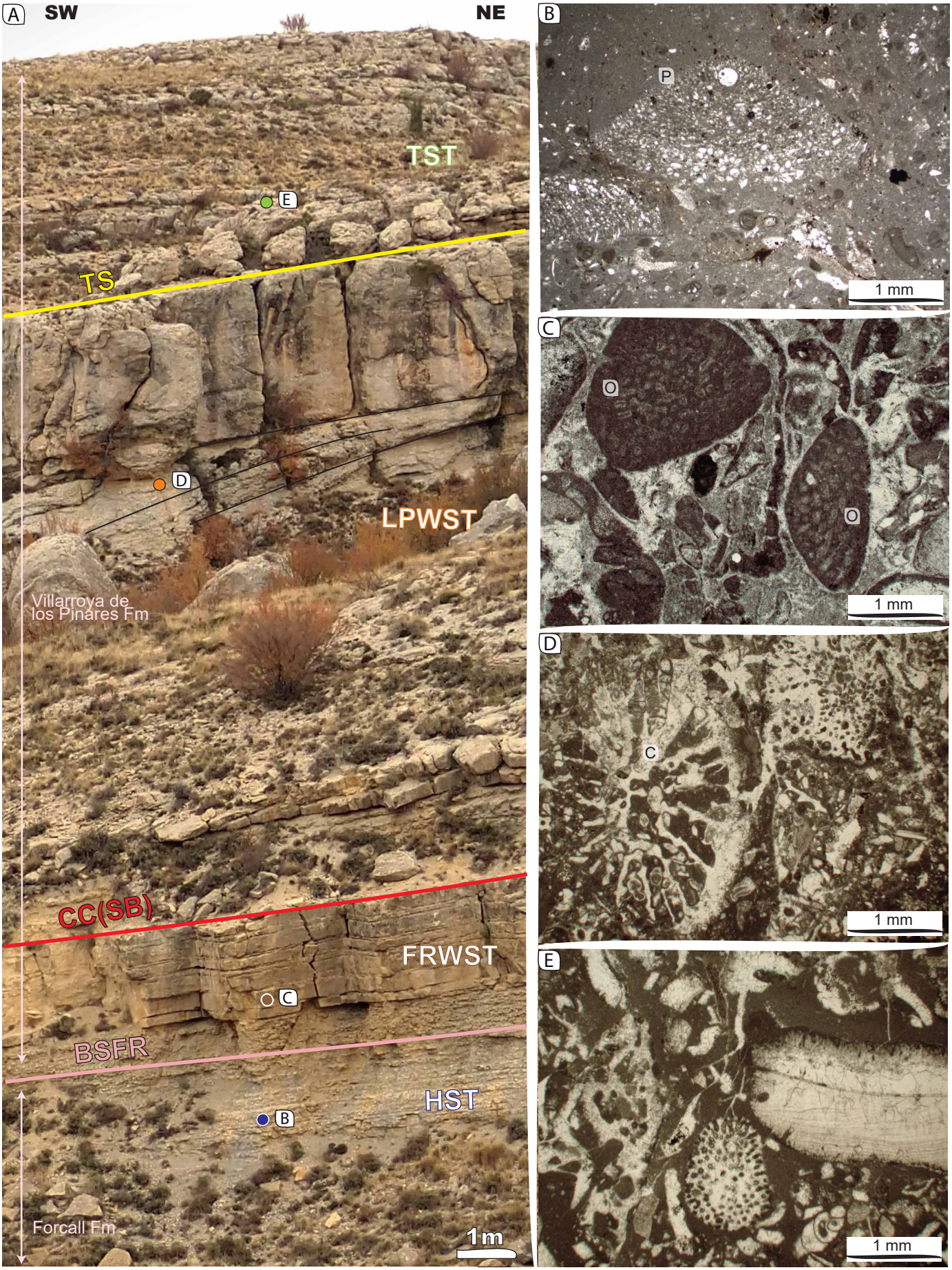

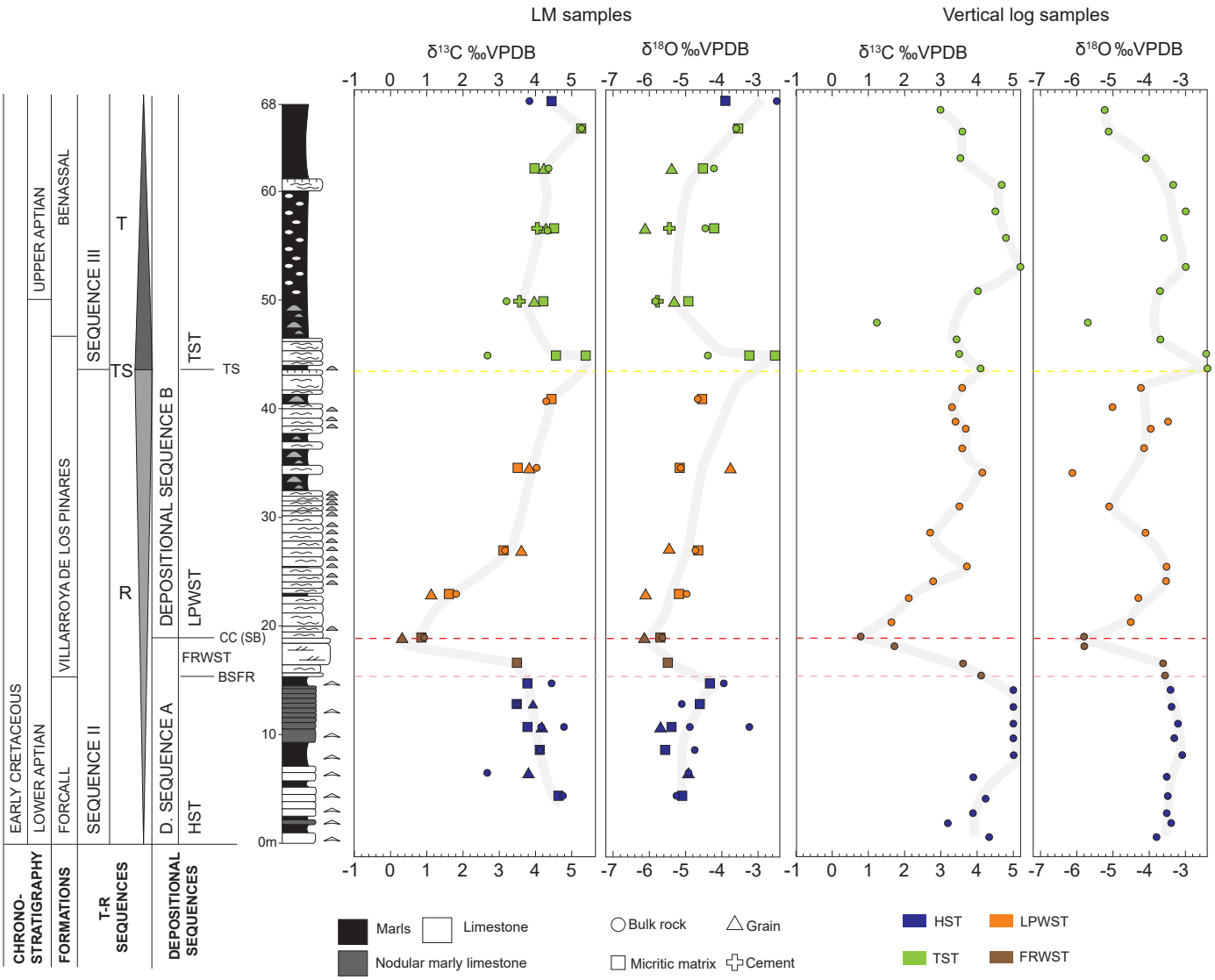

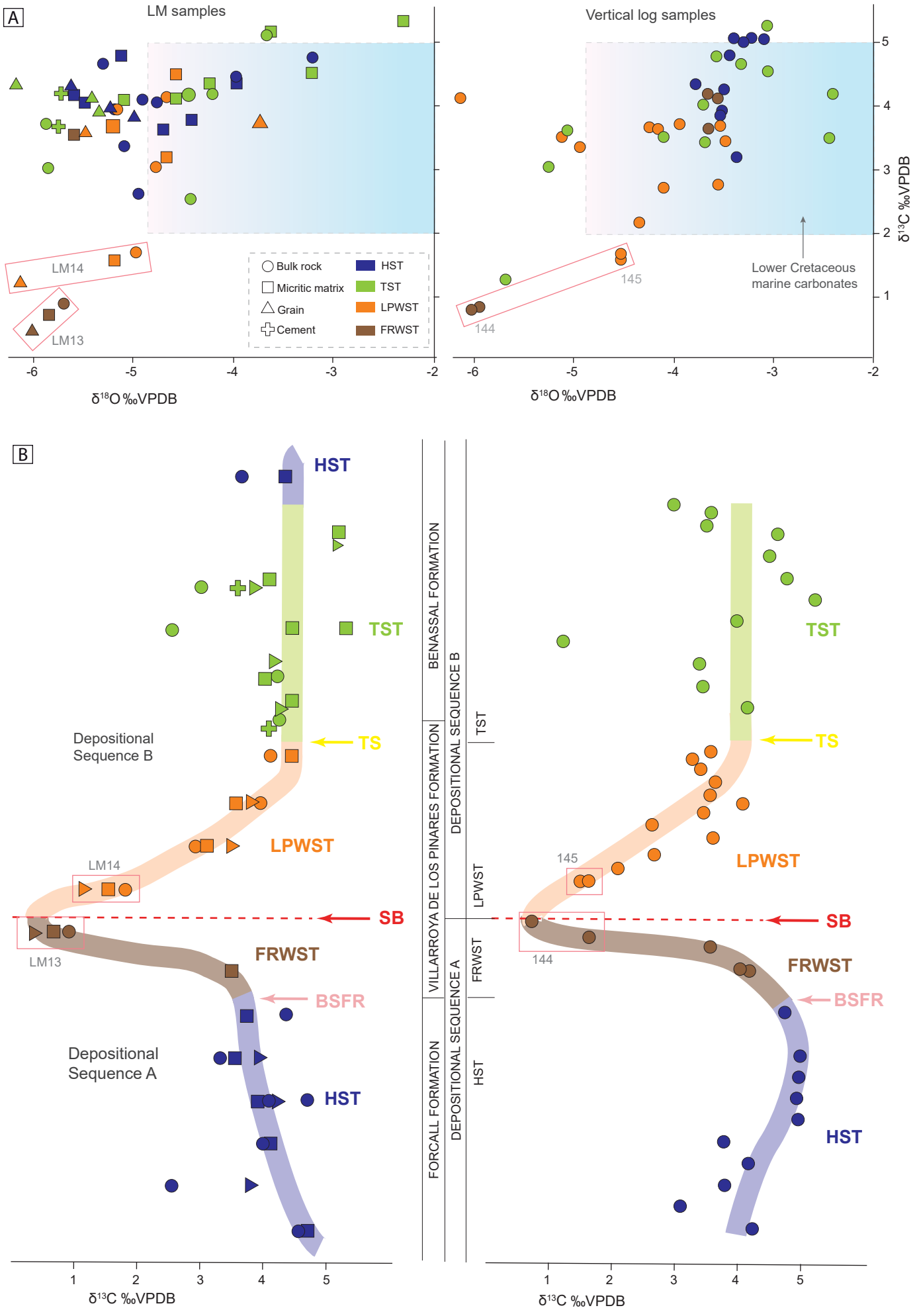

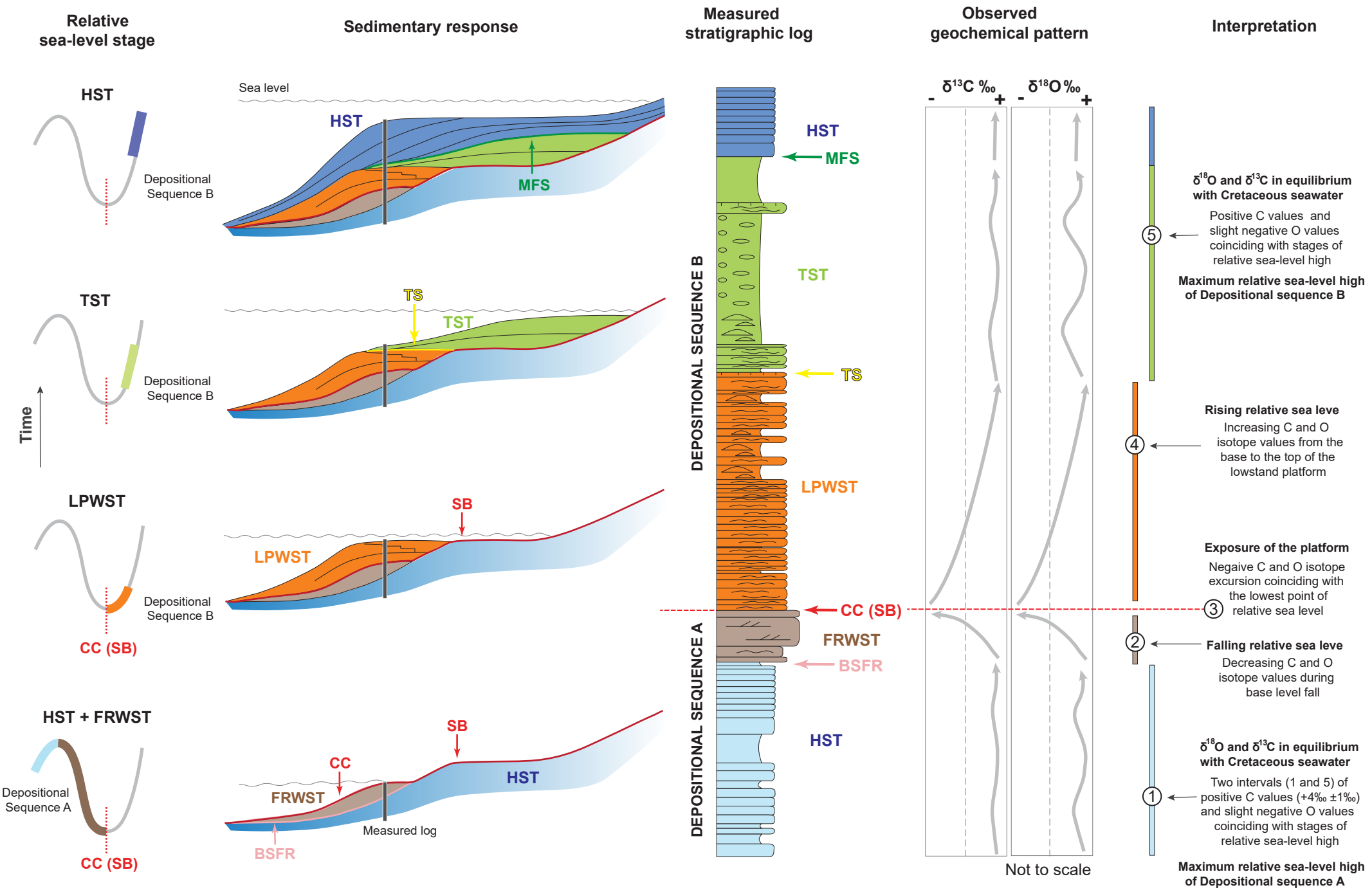

Table 1. $\delta^{13}C$ and $\delta^{18}O$ values of the studied Aptian platform carbonates. These values are arranged according to Depositional sequences A and B, their associated systems tracts, and sampling strategy (LM samples vs vertical log samples).

Depositional sequence	Systems tract	Sample reference	$\delta^{13}C$ (‰VPDB)	$\delta^{18}O$ (‰VPDB)	Sample reference	$\delta^{13}C$ (‰VPDB)	$\delta^{18}O$ (‰VPDB)
			LM samples			Vertical log samples	
		LM1-B	4.7	-5.3	131-B	4.3	-3.7
		LM1-M	4.7	-5.1	132-B	3.2	-3.4
		LM2-B	2.6	-4.9	133-B	3.9	-3.5
		LM2-G	3.8	-4.9	134-B	4.3	-3.5
		LM3-B	4.1	-4.8	135-B	3.9	-3.5
		LM3-M	4.2	-5.6	136-B	5.1	-3.1
		LM4-B	4.1	-4.9	137-B	5.0	-3.3
		LM4-B	4.7	-3.2	138-B	5.1	-3.2
A	HST	LM4-G	4.2	-5.7	139-B	5.1	-3.4
		LM4-M	4.1	-5.5	140-B	4.8	-3.4
		LM5-B	3.4	-5.1			
		LM5-G	3.9	-5.1	141a-B	4.2	-3.7
		LM5-M	3.6	-4.7	141b-B	4.1	-3.6
		LM12-B	4.4	-3.9	142-B	3.6	-3.6
		LM12-M	3,8	-4.4	143-B	1.7	-5.8
		LM15-M	3.5	-5.6	144a-B	0.8	-6.0
		LM13-B	0.9	-5.7	144b-B	0.8	-5.9
A	FRWST	LM13-M	0.7	-5.8	145a-B	1.6	-4.5
		LM13-M+G	0.5	-6.0	145b-B	1.6	-4.5
		LM14-B	1.7	-4.9	146-B	2.2	-4.3
		LM14-G	1.2	-6.1	147-B	2.8	-3.6
		LM14-M	1.6	-5.2	148-B	3.7	-3.5
		LM10-B	3.0	-4.8	149-B	2.7	-4.1
		LM10-G	3.5	-5.5	150-B	3.5	-5.1
B	LPWST	LM10-M	3.2	-4.7	157-B	4.1	-6.1
		LM11-B	3.9	-5.2	158-B	3.6	-4.2
		LM11-G	3.7	-3.7	159-B	3.7	-4.0
		LM11-M	3.7	-5.2	160-B	3.4	-3.5
		LM8-B	4.1	-4.7	161-B	3.4	-5.0
		LM8-M	4.5	-4.6	162-B	3.6	-4.2
		LM9-B	4.2	-4.5			
		LM9-CC(AH)	4.2	-5.7			
		LM9-G	4.3	-6.2			
		LM9-M	4.3	-4.2	163-B	4.2	-2.4
		LM16-B	4.2	-4.2	164-B	3.5	-2.4
		LM16-G	4.1	-5.4	165-B	3.4	-3.7
B	TST	LM16-M	4.1	-4.6	166-B	1.3	-5.7
		LM6-B	2.5	-4.4	167-B	4.0	-3.7
		LM6-M1	5.3	-2.3	168-B	5.2	-3.1
		LM6-M2	4.5	-3.2	169-B	4.8	-3.6

		LM7-B	3.7	-5.9	170-B	4.5	-3.1
		LM7-B	3.0	-5.9	171-B	4.7	-3.3
		LM7-CC	3.7	-5.8	172-B	3.5	-4.1
		LM7-G	3.9	-5.3	173-B	3.6	-5.1
		LM7-M	4.0	-5.1	174-B	3.2	-5.3
		LM17-B	5.1	-3.7			
		LM17-M	5.2	-3.6			
B	HST	LM18-B	3.6	-1.8			
		LM18-M	4.4	-3.9			